Large Deflection Aeroelasticity and Aeroelastic Lifting Line Theory for Examination of Aerodynamic Effects and Nonlinear Limit Cycle Oscillations

Nhan Nguyen *
NASA Ames Research Center, Moffett Field, CA 94035
Eric Ting †
NASA Ames Research Center, Moffett Field, CA 94035

This paper investigates the effects of nonlinear large deflection bending on the aerodynamic performance and aeroelasticity of a high aspect ratio flexible wing. A nonlinear large deflection theory is developed for aeroelasticity to account for large deflection bending. An analysis is conducted to compare the nonlinear bending theory with the linear bending theory. The results show that the nonlinear bending theory is length-preserving whereas the linear bending theory causes a non-physical effect of lengthening of the wing structure under the no axial load condition. A modified lifting line theory is developed to compute the lift and drag coefficients of a wing structure undergoing a large bending deflection. The lift and and drag coefficients are more accurately estimated by the nonlinear bending theory due to its length-preserving property. The nonlinear bending theory yields a lower lift and higher induced drag than the linear bending theory. The nonlinear large deflection bending also can affect the structural dynamics of a high aspect ratio wing significantly. Limit cycle oscillations are a nonlinear phenomenon which arises from geometric nonlinearity and other sources of nonlinearities. Large deflection can manifest itself in limit cycle oscillations whereby linear flutter behaviors can result in an increase in the bending deflection up to a point where the geometric nonlinearity due to the large deflection begins to set in that results in limit cycle oscillations.

I. Introduction

Modern aircraft are increasingly designed to be highly aerodynamically efficient in order to reduce the fuel consumption, hence operating cost of modern airlines. To achieve this goal, the aircraft industry has been adopting a high aspect ratio wing design with the composite construction in modern aircraft. Aircraft design concepts that take advantage of wing flexibility to increase aerodynamic performance and maneuverability have been investigated. By twisting a wing structure, an aerodynamic moment can be generated to enable an aircraft to execute a maneuver in place of the use of traditional flight control surfaces. For example, a rolling moment can be induced by twisting the left and right wings in the opposite direction. Similarly, a pitching moment can be generated by twisting both wings in the same direction. Wing twisting or warping for flight control is not a new concept and was used in the Wright Flyer in the 1903. The U.S. Air Force conducted the Active Flexible Wing program in the 1980's and 1990's to explore the potential use of leading edge slats and trailing edge flaps to increase the control effectiveness of F-16 aircraft for high speed maneuvers.[1] In the 2000's, the Active Aeroelastic Wing research program also investigated a similar technology to induce wing twist in order to improve roll maneuverability of a modified F/A-18 aircraft.[2] Wing shaping control concepts for drag reduction are being studied by NASA to leverage wing flexibility for aerodynamic performance.[3,4] By re-twisting a flexible wing and using variable camber aerodynamic flight control surfaces, aircraft wings can have the mission-adaptive capability to optimize L/D throughout a flight envelope.[5] In recognition of the role of aeroelasticity on aircraft performance and dynamics, NASA Advanced Air Transport Technology

*NASA Ames Research Center, Research Scientist, AIAA Associate Fellow, nhan.t.nguyen@nasa.gov
†NASA Ames Research Center, Research Engineer, eric.b.ting@nasa.gov

(AATT) project is conducting research in the area of Performance Adaptive Aeroelastic Wing (PAAW). This research develops concepts such as the variable camber continuous trailing edge flap (VCCTEF) to enable wing shaping control for aerodynamic performance and dynamics.[3,6]

Nonlinear large deflections of lifting surfaces can interact with aerodynamic forces to create aeroelastic coupling that can affect aircraft performance and dynamic stability. Understanding these effects can improve the prediction of aircraft performance and provide an insight into how to design an aerodynamically efficient high aspect ratio flexible wing. Limit cycle oscillations (LCO) are a nonlinear phenomenon which arises from geometric nonlinearity and other sources of nonlinearities. Large deflection can manifest itself in limit cycle oscillations whereby linear flutter behaviors can result in an increase in the bending deflection up to a point where the geometric nonlinearity due to the large deflection begins to set in that could lead to LCO.

This paper develops large deflection theory and modified aeroelastic lifting line theory to examine the effects of large deflection on aerodynamics. In addition, the paper will examine the dynamic response of a flexible high aspect ratio wing to investigate the existence of LCO due to large deflection.

II. Nonlinear Large Bending Deflection Strain Analysis

To analyze the nonlinear large bending deflection effect, we perform a strain analysis. Toward that end, consider an airfoil section on the left wing as shown in Fig. 1 undergoing a combined axial, bending, and torsional displacement field. Let (x, y, z) be the undeformed coordinates of point Q on a wing airfoil section in the reference frame D defined by unit vectors $(\mathbf{d}_1, \mathbf{d}_2, \mathbf{d}_3)$. Let $\mathbf{p}_0 = x\mathbf{d}_1$ be a position vector along the elastic axis. Then, point Q is defined by a position vector $\mathbf{p} = \mathbf{p}_0 + \mathbf{q}$ where $\mathbf{q} = y\mathbf{d}_2 + z\mathbf{d}_3$ defines point Q in the $y - z$ plane from the elastic axis. Then, the undeformed local airfoil coordinates of point Q are

$$\begin{bmatrix} y \\ z \end{bmatrix} = \begin{bmatrix} \cos\gamma & -\sin\gamma \\ \sin\gamma & \cos\gamma \end{bmatrix} \begin{bmatrix} \eta \\ \xi \end{bmatrix} \tag{1}$$

where η and ξ are local airfoil coordinates, and γ is the wing section pre-twist angle, positive nose-down.[11,12]

Differentiating y and z with respect to x gives

$$\begin{bmatrix} y_x \\ z_x \end{bmatrix} = \gamma' \begin{bmatrix} -\sin\gamma & -\cos\gamma \\ \cos\gamma & -\sin\gamma \end{bmatrix} \begin{bmatrix} \eta \\ \xi \end{bmatrix} = \begin{bmatrix} -z\gamma' \\ y\gamma' \end{bmatrix} \tag{2}$$

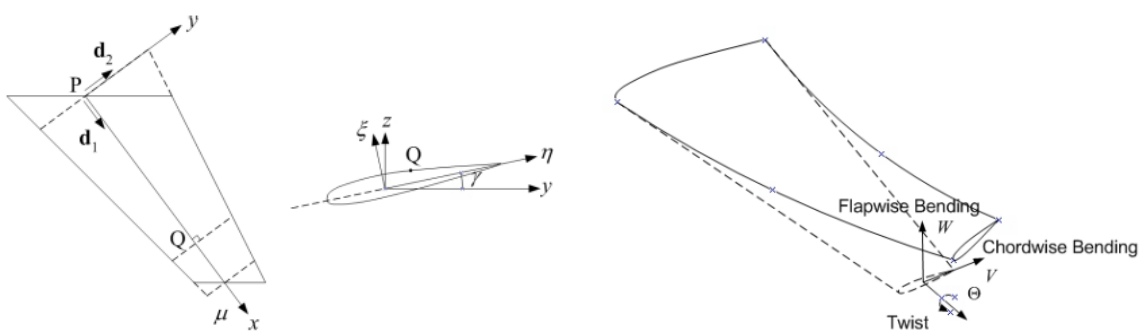

Figure 1. Left Wing Reference Frame of Wing in Combined Bending-Torsion

Let Θ be a torsional twist angle about the x-axis, positive nose-down. Let W and V be flapwise and chordwise bending deflections of point Q, respectively, and W is allowed to be large relative to V. Let U be the axial displacement of point Q. Then, the displacement and rotation vectors due to the elastic deformation can be expressed as

$$\mathbf{r} = U\mathbf{d}_1 + V\mathbf{d}_2 + W\mathbf{d}_3 \tag{3}$$

$$\boldsymbol{\phi} = \Theta\mathbf{d}_1 - \sin^{-1} W_s\mathbf{d}_2 + V_x\mathbf{d}_3 \tag{4}$$

where the subscripts x and s denote the partial derivatives of W and V with respect to x and the arc length s. Note that the term $\sin^{-1} W_s$ represents the rotation angle due to the large flapwise bending with respect to the arc length. If W_s is small, then the usual approximation $\sin^{-1} W_s \approx W_x$ applies. Otherwise, $W_x = W_s s_x$ applies where

$$s_x = \frac{ds}{dx} = \sqrt{1 + y_x^2 + z_x^2} = \sqrt{1 + (y^2 + z^2)(\gamma')^2} \tag{5}$$

Let (x_1, y_1, z_1) be the deformed coordinates of point Q on the airfoil in the reference frame D and $\mathbf{p}_1 = x_1\mathbf{d}_1 + y_1\mathbf{d}_2 + z_1\mathbf{d}_3$ be its position vector. Then the coordinates (x_1, y_1, z_1) are computed as

$$\mathbf{p}_1 = \mathbf{p} + \mathbf{r} + \boldsymbol{\phi} \times \mathbf{q} \tag{6}$$

where

$$\begin{bmatrix} x_1 \\ y_1 \\ z_1 \end{bmatrix} = \begin{bmatrix} x + U - yV_x - z\sin^{-1} W_s \\ y + V - z\Theta \\ z + W + y\Theta \end{bmatrix} \tag{7}$$

Differentiating x_1, y_1, and z_1 with respect to x yields

$$\begin{bmatrix} x_{1,x} \\ y_{1,x} \\ z_{1,x} \end{bmatrix} = \begin{bmatrix} 1 + U_x - yV_{xx} + z\gamma' V_x - z\frac{W_{ss}s_x}{\sqrt{1-W_s^2}} - y\gamma' \sin^{-1} W_x \\ -z\gamma' + V_x - z\Theta_x - y\gamma'\Theta \\ y\gamma' + \sin^{-1} W_x + y\Theta_x - z\gamma'\Theta \end{bmatrix} \tag{8}$$

Note that the term $\frac{W_{ss}}{\sqrt{1-W_s^2}}$ represents the physical curvature of the nonlinear bending with a large deflection. This term is consistent with the nonlinear bending curvature formula by Hodges.[16] Other authors[14,15] have used the curvature formula $\frac{W_{ss}}{(1+W_s^2)^{\frac{3}{2}}}$ based on the elementary calculus which is sometimes mistaken as the physical curvature of a beam as stated by Hodges.[16] The curvature formula $\frac{W_{ss}}{\sqrt{1-W_s^2}}$ can be used in the undeformed coordinates whereas the curvature formula $\frac{W_{ss}}{(1+W_s^2)^{\frac{3}{2}}}$ must be used in the deformed coordinates which are impractical for implementation.

Neglecting the transverse shear effect, the longitudinal strain is computed as[12]

$$\epsilon = \frac{ds_1 - ds}{ds} = \frac{s_{1,x}}{s_x} - 1 \tag{9}$$

where

$$\begin{aligned} s_{1,x} &= \sqrt{x_{1,x}^2 + y_{1,x}^2 + z_{1,x}^2} \\ &= \sqrt{s_x^2 + 2U_x - 2yV_{xx} - 2z\frac{W_{ss}s_x}{\sqrt{1-W_s^2}} + 2(y^2+z^2)\gamma'\Theta_x + (x_{1,x}-1)^2 + (y_{1,x}+z\gamma')^2 + (z_{1,x}-y\gamma')^2} \end{aligned} \tag{10}$$

$s_{1,x}$ is approximated by a Taylor series as

$$s_{1,x} \approx s_x + U_x - yV_{xx} - z\frac{W_{ss}s_x}{\sqrt{1-W_s^2}} + \left(y^2+z^2\right)\gamma'\Theta_x + \frac{(x_{1,x}-1)^2 + \left(y_{1,x}+z\gamma'\right)^2 + \left(z_{1,x}-y\gamma'\right)^2}{2} + \cdots \tag{11}$$

The slope of the twist angle γ' can play a significant role in structures with large twists such as turbomachinery blades. For aircraft wings, this effect is negligible and therefore can be neglected. Thus, for a small wing twist angle slope, $\gamma' \approx 0$ and $s_x \approx 1$. Then $W_s \approx W_x$ and $W_{ss} \approx W_{xx}$. Neglecting all the nonlinear terms associated with the chordwise bending, the longitudinal strain is then obtained as

$$\begin{aligned} \epsilon = U_x - yV_{xx} - z(1+U_x)\frac{W_{xx}}{\sqrt{1-W_x^2}} + \frac{1}{2}U_x^2 + \frac{1}{2}\left(\sin^{-1} W_x\right)^2 + \frac{1}{2}\left(y^2+z^2\right)\Theta_x^2 + \frac{1}{2}z^2\frac{W_{xx}^2}{1-W_x^2} \\ + y\sin^{-1} W_x\Theta_x \end{aligned} \tag{12}$$

Assuming that the neutral axis of a wing section passes through the elastic axis, then the axial force and moments acting on a wing are evaluated as[7]

$$P_x = \int E\epsilon dA = EAU_x + \frac{1}{2}EA\left[U_x^2 + \left(\sin^{-1} W_x\right)^2\right] + \frac{1}{2}EI_{xx}\Theta_x^2 + \frac{1}{2}EI_{yy}\frac{W_{xx}^2}{1-W_x^2} \tag{13}$$

$$\begin{aligned} M_x = GJ\Theta_x + \int E\epsilon\left(y^2+z^2\right)\Theta_x dA = \Bigg\{ & GJ + EI_{xx}U_x - \left(1+U_x\right)EB_2\frac{W_{xx}}{\sqrt{1-W_x^2}} \\ & + \frac{1}{2}EI_{xx}\left[U_x^2 + \left(\sin^{-1} W_x\right)^2\right] + \frac{1}{2}EB_1\Theta_x^2 + \frac{1}{2}EB_5\frac{W_{xx}^2}{1-W_x^2} + EB_3\sin^{-1} W_x\Theta_x \Bigg\}\Theta_x \end{aligned} \tag{14}$$

$$M_y = -\int E\epsilon z dA = \left(1+U_x\right)EI_{yy}\frac{W_{xx}}{\sqrt{1-W_x^2}} - \frac{1}{2}EB_2\Theta_x^2 - \frac{1}{2}EB_8\frac{W_{xx}^2}{1-W_x^2} \tag{15}$$

$$M_z = -\int E\epsilon y dA = EI_{zz}V_{xx} - \frac{1}{2}EB_3\Theta_x^2 - \frac{1}{2}EB_9\frac{W_{xx}^2}{1-W_x^2} - EI_{zz}\sin^{-1} W_x\Theta_x \tag{16}$$

where E is the Young's modulus, G is the shear modulus, A is the tensile area, J is the torsional constant, and B_i, $i = 1, 2, \ldots, 10$ are defined as

$$\begin{bmatrix} B_1 \\ B_2 \\ B_3 \\ B_4 \\ B_5 \\ B_6 \\ B_7 \\ B_8 \\ B_9 \\ B_{10} \end{bmatrix} = \int \begin{bmatrix} \left(y^2+z^2\right)^2 \\ z\left(y^2+z^2\right) \\ y\left(y^2+z^2\right) \\ y^2\left(y^2+z^2\right) \\ z^2\left(y^2+z^2\right) \\ yz\left(y^2+z^2\right) \\ y^2 z \\ z^3 \\ yz^2 \\ y^3 \end{bmatrix} dA \tag{17}$$

For a rectangular wing box structure with the neutral axis in coincidence with the elastic axis, the constants B_1, B_4, and B_5 are generally much larger than the other constants B_i, $i \neq 1, 4, 5$ and can be approximated as

$$\begin{bmatrix} B_1 \\ B_4 \\ B_5 \end{bmatrix} \approx \frac{1}{A}\begin{bmatrix} I_{xx}^2 \\ I_{xx}I_{zz} \\ I_{xx}I_{yy} \end{bmatrix} \tag{18}$$

Assuming that the nonlinear contributions of the chordwise bending deflection are small and neglecting the cross-product inertia I_{yz} and the small constants B_i, $i \neq 1, 4, 5$, then the following simplification can be made:

$$M_x = \left(GJ + P_x r_k^2\right)\Theta_x \tag{19}$$

$$M_y = \left(1+U_x\right)EI_{yy}\frac{W_{xx}}{\sqrt{1-W_x^2}} \tag{20}$$

$$M_z = EI_{zz}V_{xx} - EI_{zz}\sin^{-1} W_x\Theta_x \tag{21}$$

where $r_k = \sqrt{\frac{I_{xx}}{A}}$ is the radius of gyration.

Note that the signs of the moments are defined in the positive deflection sense such that

$$\mathbf{M} = M_x\mathbf{d}_1 - M_y\mathbf{d}_2 + M_z\mathbf{d}_3 \tag{22}$$

The resulting equilibrium equations are given by[7]

$$\frac{\partial}{\partial x}\begin{bmatrix} P_x \\ P_y \\ P_z \end{bmatrix} = -\begin{bmatrix} f_x \\ f_y \\ f_z \end{bmatrix} \tag{23}$$

$$\frac{\partial}{\partial x}\begin{bmatrix} M_x \\ M_y \\ M_z \end{bmatrix} = \begin{bmatrix} P_y W_x - P_z V_x - m_x \\ P_x W_x - P_z + m_y \\ P_x V_x - P_y - m_z \end{bmatrix} \tag{24}$$

These equations become

$$\frac{\partial M_x}{\partial x} + \underbrace{\left(\frac{\partial M_z}{\partial x} - P_x V_x + m_z\right)}_{0} W_x - \underbrace{\left(\frac{\partial M_y}{\partial x} - P_x W_x - m_y\right)}_{0} V_x + m_x = 0 \tag{25}$$

$$\frac{\partial^2 M_y}{\partial x^2} - \frac{\partial\left(P_x W_x\right)}{\partial x} - \frac{\partial m_y}{\partial x} - f_z = 0 \tag{26}$$

$$\frac{\partial^2 M_z}{\partial x^2} - \frac{\partial\left(P_x V_x\right)}{\partial x} + \frac{\partial m_z}{\partial x} - f_y = 0 \tag{27}$$

The resulting nonlinear equations are obtained as

$$\frac{\partial}{\partial x}\left\{EAU_x + \frac{1}{2}EA\left[U_x^2 + \left(\sin^{-1} W_x\right)^2\right] + \frac{1}{2}EI_{xx}\Theta_x^2 + \frac{1}{2}EI_{yy}\frac{W_{xx}^2}{1 - W_x^2}\right\} = -f_x \tag{28}$$

$$\frac{\partial}{\partial x}\left[\left(GJ + P_x r_k^2\right)\Theta_x\right] = -m_x \tag{29}$$

$$\frac{\partial^2}{\partial x^2}\left[\left(1 + U_x\right) EI_{yy}\frac{W_{xx}}{\sqrt{1 - W_x^2}}\right] - \frac{\partial\left(P_x W_x\right)}{\partial x} = f_z + \frac{\partial m_y}{\partial x} \tag{30}$$

$$\frac{\partial^2}{\partial x^2}\left(EI_{zz}V_{xx} - EI_{zz}\sin^{-1} W_x \Theta_x\right) - \frac{\partial\left(P_x V_x\right)}{\partial x} = f_y - \frac{\partial m_z}{\partial x} \tag{31}$$

III. Inertial Force Analysis

The relative velocity of the air approaching a wing section includes the contribution from the wing elastic deflection that results in changes in the local angle of attack. Since aerodynamic forces and moments are dependent on the local angle of attack, the wing aeroelastic deflections will generate additional elastic forces and moments. The local angle of attack depends on the relative approaching air velocity as well as the rotation angle $\boldsymbol{\phi}$ from Eq. (4). The relative air velocity in turn also depends on the deflection-induced velocity. The velocity at point Q due to the aircraft velocity and angular velocity in the reference frame D is computed as

$$\begin{aligned} \mathbf{v}_Q &= \bar{\mathbf{v}} + \boldsymbol{\omega} \times \mathbf{r} = \left(u\mathbf{b}_1 + v\mathbf{b}_2 + w\mathbf{b}_3\right) + \left(p\mathbf{b}_1 + q\mathbf{b}_2 + r\mathbf{b}_3\right) \times \left(-x_a\mathbf{b}_1 - y_a\mathbf{b}_2 - z_a\mathbf{b}_3\right) \\ &= \left(u + ry_a - qz_a\right)\mathbf{b}_1 + \left(v - rx_a + pz_a\right)\mathbf{b}_2 + \left(w + qx_a - py_a\right)\mathbf{b}_3 \\ &= x_t\mathbf{d}_1 + y_t\mathbf{d}_2 + z_t\mathbf{d}_3 \end{aligned} \tag{32}$$

where (u, v, w) are the aircraft velocity components, (p, q, r) are aircraft angular velocity components in the roll, pitch, and yaw axes, and (x_a, y_a, z_a) is the coordinate of point Q in the aircraft body-fixed reference frame B relative to the aircraft CG (center of gravity) such that x_a is positive when point Q is aft of the aircraft CG, y_a is positive when point Q is toward the left wing from the aircraft CG, and z_a is positive when point Q is above the aircraft CG.

The coordinate transformation between the reference frame B defined by the unit vectors $(\mathbf{b}_1, \mathbf{b}_2, \mathbf{b}_3)$ and D is given by

$$\begin{bmatrix} \mathbf{b}_1 \\ \mathbf{b}_2 \\ \mathbf{b}_3 \end{bmatrix} = \begin{bmatrix} -\sin\Lambda\cos\Gamma & -\cos\Lambda & \sin\Lambda\sin\Gamma \\ -\cos\Lambda\cos\Gamma & \sin\Lambda & \cos\Lambda\sin\Gamma \\ -\sin\Gamma & 0 & -\cos\Gamma \end{bmatrix}\begin{bmatrix} \mathbf{d}_1 \\ \mathbf{d}_2 \\ \mathbf{d}_3 \end{bmatrix} \tag{33}$$

where Γ is the wing dihedral angle.

Consider a trim problem when $\beta = 0$, $p = q = r = 0$ for steady-state aerodynamics. For simplicity, we assume $\Gamma = 0$. Then,

$$\begin{bmatrix} x_t \\ y_t \\ z_t \end{bmatrix} = \begin{bmatrix} -u \sin\Lambda \\ -u \cos\Lambda \\ -w \end{bmatrix} \tag{34}$$

The local velocity at point Q due to the aeroelastic deflections is obtained as

$$\begin{bmatrix} x_{1,t} \\ y_{1,t} \\ z_{1,t} \end{bmatrix} = \begin{bmatrix} x_t + U_t - yV_{xt} - z\frac{W_{xt}}{\sqrt{1-W_x^2}} \\ y_t + V_t - z\Theta_t \\ z_t + W_t + y\Theta_t \end{bmatrix} \tag{35}$$

When the aircraft is trimmed, $\dot{u} = \dot{w} = 0$. Then, the acceleration of point Q due to the aeroelastic deflections is computed as

$$\begin{bmatrix} x_{1,tt} \\ y_{1,tt} \\ z_{1,tt} \end{bmatrix} \approx \begin{bmatrix} U_{tt} - yV_{xtt} - z\frac{W_{xtt}}{\sqrt{1-W_x^2}} \\ V_{tt} - z\Theta_{tt} \\ W_{tt} + y\Theta_{tt} \end{bmatrix} \tag{36}$$

The inertial force is evaluated as

$$\begin{bmatrix} f_x^i \\ f_y^i \\ f_z^i \end{bmatrix} = -\int \begin{bmatrix} x_{1,tt} \\ y_{1,tt} \\ z_{1,tt} \end{bmatrix} \rho dA = -\rho A \begin{bmatrix} U_{tt} - e_{cg}V_{xtt} \\ V_{tt} \\ W_{tt} + e_{cg}\Theta_{tt} \end{bmatrix} \tag{37}$$

where e_{cg} is the offset of the center of mass from the elastic axis (positive with the center of mass aft of the elastic axis).

The inertial moment is evaluated as

$$\begin{bmatrix} m_x^i \\ m_y^i \\ m_z^i \end{bmatrix} = -\int \begin{bmatrix} yz_{1,tt} - zy_{1,tt} \\ zx_{1,tt} \\ -yx_{1,tt} \end{bmatrix} \rho dA = -\begin{bmatrix} \rho A e_{cg} W_{tt} + \rho I_{xx}\Theta_{tt} \\ -\rho I_{yy}\frac{W_{xtt}}{\sqrt{1-W_x^2}} \\ -\rho A e_{cg} U_{tt} + \rho I_{zz} V_{xtt} \end{bmatrix} \tag{38}$$

The structural dynamic equations are now expressed as

$$\frac{\partial}{\partial x}\left\{EAU_x + \frac{1}{2}EA\left[U_x^2 + \left(\sin^{-1} W_x\right)^2\right] + \frac{1}{2}EI_{xx}\Theta_x^2 + \frac{1}{2}EI_{yy}\frac{W_{xx}^2}{1-W_x^2}\right\} = \rho A\left(U_{tt} - e_{cg}V_{xtt}\right) - f_x^a \tag{39}$$

$$\frac{\partial}{\partial x}\left[\left(GJ + P_x r_k^2\right)\Theta_x\right] = \rho A e_{cg} W_{tt} + \rho I_{xx}\Theta_{tt} - m_x^a \tag{40}$$

$$\frac{\partial^2}{\partial x^2}\left[\frac{(1+U_x)\,EI_{yy}W_{xx}}{\sqrt{1-W_x^2}}\right] - \frac{\partial\left(P_x W_x\right)}{\partial x} = -\rho A\left(W_{tt} + e_{cg}\Theta_{tt}\right) + \frac{\partial}{\partial x}\left(\rho I_{yy}\frac{W_{xtt}}{\sqrt{1-W_x^2}}\right) + f_z^a + \frac{\partial m_y^a}{\partial x} \tag{41}$$

$$\frac{\partial^2}{\partial x^2}\left(EI_{zz}V_{xx} - EI_{zz}\sin^{-1} W_x\Theta_x\right) - \frac{\partial\left(P_x V_x\right)}{\partial x} = -\rho A V_{tt} + \frac{\partial}{\partial x}\left(-\rho A e_{cg} U_{tt} + \rho I_{zz} V_{xtt}\right) + f_y^a - \frac{\partial m_z^a}{\partial x} \tag{42}$$

IV. Aeroelastic Analysis

The forces and moments on the right hand side of Eqs. (28) - (31) also include aerodynamic and gravity forces and moments. In order to compute the aerodynamic forces and moments of a flexible wing structure, static aeroelasticity must be considered.

Neglecting the rotation due to the chordwise bending and making the small angle assumption for Θ, the velocity of point Q is transformed from the reference frame D to the airfoil local coordinate reference frame

defined by (μ, η, ξ) as follows:

$$\begin{bmatrix} v_\mu \\ v_\eta \\ v_\xi \end{bmatrix} = \begin{bmatrix} 1 & 0 & 0 \\ 0 & 1 & \Theta \\ 0 & -\Theta & 1 \end{bmatrix} \begin{bmatrix} \sqrt{1-W_x^2} & 0 & W_x \\ 0 & 1 & 0 \\ -W_x & 0 & \sqrt{1-W_x^2} \end{bmatrix} \begin{bmatrix} x_{1,t} \\ y_{1,t} \\ z_{1,t} \end{bmatrix}$$
$$= \begin{bmatrix} x_{1,t}\sqrt{1-W_x^2} + z_{1,t}W_x \\ -x_{1,t}\Theta W_x + y_{1,t} + z_{1,t}\Theta\sqrt{1-W_x^2} \\ -x_{1,t}W_x - y_{1,t}\Theta + z_{1,t}\sqrt{1-W_x^2} \end{bmatrix} \tag{43}$$

For a small angle of attack, the usual assumption of $\alpha = \frac{w}{u}$ is valid, but if the rotation angle due to the flapwise bending is large, then some accuracy in the small angle of attack assumption may be suffered. Therefore, the exact angle of attack definition $\alpha = \tan^{-1}\frac{w}{u}$ is used. Then, the local aeroelastic angle of attack on the airfoil section due to the velocity components v_η and v_ξ defined with respect to the elastic axis is computed as

$$\alpha_c = \tan^{-1}\frac{v_\xi}{v_\eta} \approx \tan^{-1}\frac{\bar{v}_\xi}{\bar{v}_\eta} + \frac{\frac{\Delta v_\xi}{\bar{v}_\eta} - \frac{\bar{v}_\xi \Delta v_\eta}{\bar{v}_\eta^2}}{1+\left(\frac{\bar{v}_\xi}{\bar{v}_\eta}\right)^2} \tag{44}$$

where

$$\bar{v}_\xi = -w \tag{45}$$

$$\Delta v_\xi = -\left(-u\sin\Lambda + U_t - yV_{xt}\right)W_x - \left(-u\cos\Lambda + V_t\right)\Theta + \left(-w + W_t + y\Theta_t\right)\sqrt{1-W_x^2} + w \tag{46}$$

$$\bar{v}_\eta = -u\cos\Lambda \tag{47}$$

$$\Delta v_\eta = -\left(-u\sin\Lambda + U_t - yV_{xt}\right)\Theta W_x + V_t + \left(-w + W_t + y\Theta_t\right)\Theta\sqrt{1-W_x^2} \tag{48}$$

Then,

$$\begin{aligned} \alpha_c = {} & \tan^{-1}\left(\frac{w}{u\cos\Lambda}\right) \\ & + \frac{1}{1+\frac{w^2}{u^2\cos^2\Lambda}} \frac{-\left(-u\sin\Lambda + U_t - yV_{xt}\right)W_x - \left(-u\cos\Lambda + V_t\right)\Theta + \left(-w + W_t + y\Theta_t\right)\sqrt{1-W_x^2} + w}{-u\cos\Lambda} \\ & - \frac{1}{1+\frac{w^2}{u^2\cos^2\Lambda}} \frac{-w\left[-\left(-u\sin\Lambda + U_t - yV_{xt}\right)\Theta W_x + V_t + \left(-w + W_t + y\Theta_t\right)\Theta\sqrt{1-W_x^2}\right]}{u^2\cos^2\Lambda} \end{aligned} \tag{49}$$

Using the Taylor series approximation of $\sqrt{1-W_x^2} \approx 1 - \frac{W_x^2}{2}$ and $\tan^{-1}\left(\frac{\tan\alpha}{\cos\Lambda}\right) \approx \frac{\tan\alpha}{\cos\Lambda}\left(1 - \frac{\tan^2\alpha}{6\cos^2\Lambda}\right) \approx \frac{\alpha}{\cos\Lambda}\left(1+\frac{\alpha^2}{6}\right)\left[1 - \frac{\alpha^2}{6\cos^2\Lambda}\left(1+\frac{\alpha^2}{6}\right)^2\right] \approx \frac{\alpha}{\cos\Lambda}\left(1 - \frac{\alpha^2}{6}\tan^2\Lambda\right)$, the local angle of attack can be expressed as

$$\alpha_c = \alpha_r + \alpha_e \tag{50}$$

where

$$\alpha_r = \frac{\alpha}{\cos\Lambda}\left(1 - \frac{\alpha^2\tan^2\Lambda}{6}\right) \tag{51}$$

is the rigid angle of attack due to the aircraft velocity and

$$\begin{aligned} \alpha_e(y) = {} & \frac{\cos\Lambda - \tan\alpha\Theta}{\cos^2\Lambda + \tan^2\alpha}\left[-\sin\Lambda W_x - \frac{\tan\alpha W_x^2}{2} - \frac{y\left(1-\frac{W_x^2}{2}\right)\Theta_t}{V_\infty} + \frac{W_x U_t}{V_\infty} - \frac{yW_xV_{xt}}{V_\infty}\right] - \Theta \\ & - \frac{\cos\Lambda}{\cos^2\Lambda + \tan^2\alpha}\frac{\left(1-\frac{W_x^2}{2}\right)W_t}{V_\infty} + \frac{\cos\Lambda\Theta + \tan\alpha}{\cos^2\Lambda + \tan^2\alpha}\frac{V_t}{V_\infty} \end{aligned} \tag{52}$$

is the elastic angle of attack due to the aeroelastic deflections. Note that the rigid angle of attack is defined with respect to the elastic axis, hence the term $\cos\Lambda$ in the denominator. For a sweptback wing, the

contribution of W_x is negative, thus effectively reduces the total aeroelastic angle of attack. The bending deflection thus creates an effective wash-out twist to reduce the local angle of attack for sweptback wings. Consequently, the trim angle of attack must be increased in order to compensate for the wash-out twist. Equation (52) for nonlinear large bending deflection should be contrasted with the following equation for linear bending deflection.

$$\alpha_e(y) = -\tan\Lambda W_x - \Theta - \frac{y\Theta_t}{V_\infty \cos\Lambda} - \frac{W_t}{V_\infty \cos\Lambda} \tag{53}$$

The aerodynamic and body forces and moments are given by

$$\begin{bmatrix} f_x^a \\ f_y^a \\ f_z^a \\ m_x^a \\ m_y^a \\ m_z^a \end{bmatrix} = \begin{bmatrix} c_D q_\infty c \sin\Lambda\cos\Lambda \\ c_D q_\infty c \cos^2\Lambda \\ c_L q_\infty c\cos\Lambda - \rho A g \\ -c_m q_\infty c^2 \cos^2\Lambda + \rho A g e_{cg} \\ c_m q_\infty c^2 \sin\Lambda\cos\Lambda \\ 0 \end{bmatrix} \tag{54}$$

where q_∞ is the dynamic pressure, c is the chord length, and g is the gravity acceleration.

The circulatory lift and pitching moment coefficients in the streamwise direction are computed from

$$c_{L_c} = \left[c_{L_0} + c_{L_\alpha}\alpha_r + C(k)\, c_{L_\alpha}\alpha_e\,(e_c\cos\Lambda)\right]\cos\Lambda \tag{55}$$

$$c_{m_c} = c_{m_{ac}} + \frac{e}{c}\left[c_{L_\alpha}\alpha_r + C(k)\, c_{L_\alpha}\alpha_e\,(e_c\cos\Lambda)\right]\cos\Lambda \tag{56}$$

where $C(k)$ is the Theodorsen's function, $k = \frac{\omega c}{2V_\infty}$ is the reduced frequency, c_{L_0} and c_{D_0} are the lift and drag coefficients at zero angle of attack, c_{L_α} is the lift curve slope, k is the drag polar parameter, $c_{m_{ac}}$ is the pitching moment coefficient at the aerodynamic center, e is the offset of the aerodynamic center from the elastic axis (positive with the aerodynamic center forward of the elastic axis), and e_c is the offset of the three-quarter chord point from the elastic axis.

The non-circulatory lift and pitching moment coefficients in the streamwise direction are given by[7]

$$c_{L_{nc}} = \frac{\pi c\cos\Lambda}{2V_\infty}\frac{\partial\alpha_e\,(e_m\cos\Lambda)}{\partial t} \tag{57}$$

$$c_{m_{nc}} = -2\pi\cos\Lambda\left[\frac{c}{16}\frac{\partial\alpha_e}{\partial\bar{y}} + \frac{c^2}{128V_\infty}\frac{\partial^2\alpha_e}{\partial\bar{y}\partial t} + \frac{e_m}{4V_\infty}\frac{\partial\alpha_e\,(e_m\cos\Lambda)}{\partial t}\right] \tag{58}$$

where $\bar{y} = \frac{y}{\cos\Lambda}$ is the airfoil coordinate in the streamwise direction, and e_m is the offset of the mid-chord point from the elastic axis.

The drag coefficient can be approximated by a quadratic relationship as follows:

$$c_{D_c} = c_{D_0} + k\left(c_{L_c} + c_{L_{nc}}\right)^2 \tag{59}$$

V. Effect of Large Deflection on Aerodynamics

Consider the case of static aeroelasticity of unswept wings for which $f_x = 0$. The aeroelastic angle of attack is reduced to

$$\alpha_c = \alpha - \frac{1-\tan\alpha\Theta}{1+\tan^2\alpha}\frac{\tan\alpha W_x^2}{2} - \Theta \tag{60}$$

For linear structures, the wing bending deflection has no effect on the wash-out twist for unswept wings. In contrast, for nonlinear structures, the contribution of the wing bending to the wash-out twist is non-zero due to the term W_x^2, although this term is small. Nonetheless, this results in a bending-torsion aeroelastic coupling even though the wings are unswept.

Since there is no applied axial force at the end of the cantilever wing, the axial displacement equation is equal to zero

$$P_x = EAU_x + \frac{1}{2}EA\left[U_x^2 + \left(\sin^{-1}W_x\right)^2\right] + \frac{1}{2}EI_{xx}\Theta_x^2 + \frac{1}{2}EI_{yy}\frac{W_{xx}^2}{1-W_x^2} = 0 \tag{61}$$

Solving for U_x from Eq. (61) yields

$$1 + U_x = \sqrt{1 - \left(\sin^{-1} W_x\right)^2 - \frac{I_{xx}}{A}\Theta_x^2 - \frac{I_{yy}}{A}\frac{W_{xx}^2}{1 - W_x^2}} \tag{62}$$

Then, the nonlinear static aeroelastic equations become

$$\frac{\partial}{\partial x}\left(GJ\Theta_x\right) + c_{L_\alpha} q_\infty ec\left(\frac{1 - \tan\alpha\Theta}{1 + \tan^2\alpha}\frac{\tan\alpha W_x^2}{2} + \Theta\right) = c_{m_r} q_\infty c^2 - mge_{cg} \tag{63}$$

$$\frac{\partial^2}{\partial x^2}\left[EI_{yy}W_{xx}\sqrt{\frac{1 - \left(\sin^{-1} W_x\right)^2 - r_k^2\Theta_x^2 - \frac{I_{yy}}{A}\frac{W_{xx}^2}{1-W_x^2}}{1 - W_x^2}}\right] + c_{L_\alpha} q_\infty c\left(\frac{1 - \tan\alpha\Theta}{1 + \tan^2\alpha}\frac{\tan\alpha W_x^2}{2} + \Theta\right) = c_{L_r} q_\infty c - mg \tag{64}$$

$$\frac{\partial^2}{\partial x^2}\left(EI_{zz}V_{xx} - EI_{zz}\sin^{-1} W_x\Theta_x\right) + \left(c_{D_\alpha} + 2c_{D_\alpha^2}\alpha\right) q_\infty c\left(\frac{1 - \tan\alpha\Theta}{1 + \tan^2\alpha}\frac{\tan\alpha W_x^2}{2} + \Theta\right) - c_{D_\alpha^2} q_\infty c\left(\frac{1 - \tan\alpha\Theta}{1 + \tan^2\alpha}\frac{\tan\alpha W_x^2}{2} - \Theta\right)^2 = c_{D_r} q_\infty c \tag{65}$$

where $c_{L_r} = c_{L_0} + c_{L_\alpha}\alpha$ is the rigid lift coefficient, $c_{D_r} = c_{D_0} + c_{D_\alpha}\alpha + c_{D_{\alpha^2}}\alpha^2$ is the rigid drag coefficient, and $c_{m_r} = c_{m_{ac}} + c_{L_r}\frac{e}{c}$ is the rigid pitching moment coefficient about the elastic axis.

If the torsional twist is small relative to the flapwise bending slope, then the nonlinear static aeroelastic equation for bending is expressed as

$$\frac{\partial^2}{\partial x^2}\left[EI_{yy}W_{xx}\sqrt{\frac{1 - \left(\sin^{-1} W_x\right)^2 - \frac{I_{yy}}{A}\frac{W_{xx}^2}{1-W_x^2}}{1 - W_x^2}}\right] + c_{L_\alpha} q_\infty c\frac{\tan\alpha W_x^2}{2\left(1 + \tan^2\alpha\right)} = c_{L_r} q_\infty c - mg \tag{66}$$

A. Aeroelastic Lifting Line Theory

For the large deflection bending of the wing structure, a modified lifting line theory is used.[16] The velocity distribution induced by a trailing vortex at $x = x_0$ is given by the Biot-Savart law according to[17]

$$\frac{d\mathbf{v}_i}{dx} = -\int \frac{\Gamma_x d\mathbf{l} \times \mathbf{r}}{4\pi\mathbf{r}^3} \tag{67}$$

where $\Gamma_x = \frac{d\Gamma}{dx}$ is the lift circulation distribution, $\mathbf{r} = (x_0 - x + U_0 - U)\,\mathbf{d}_1 - (y)\,\mathbf{d}_2 + (W_0 - W)\,\mathbf{d}_3$, and $d\mathbf{l} = dy\mathbf{d}_2$. This yields the following expression:

$$\frac{d\mathbf{v}_i}{dx} = -\int_0^\infty \frac{\Gamma_x\left[-\left(x_0 - x + U_0 - U\right)dy\mathbf{d}_3 + Wdy\mathbf{d}_1\right]}{4\pi\mathbf{r}^3} \tag{68}$$

Due to the axial displacement and bending effects, in addition to the induced downwash distribution, there also exists an induced sidewash distribution. However, the total induced sidewash for the entire trailing edge vortex sheet is zero due to the symmetry of the wing bending. Therefore, the remaining induced downwash distribution is evaluated as

$$\frac{dw_i}{dx} = \int_0^\infty \frac{\Gamma_x\left(x_0 - x + U_0 - U\right)dy}{4\pi\left[\left(x_0 - x + U_0 - U\right)^2 + y^2 + \left(W_0 - W\right)^2\right]^{\frac{3}{2}}} = -\frac{\Gamma_x\left(x_0 - x + U_0 - U\right)}{4\pi\left[\left(x_0 - x + U_0 - U\right)^2 + \left(W_0 - W\right)^2\right]} \tag{69}$$

where U_0 and W_0 is the wing axial displacement and bending deflection at $x = x_0$.

The total induced downwash at $x = x_0$ is the integral of the induced downwash distribution which is expressed as

$$w_i\left(x_0\right) = -\int_{-\frac{b}{2}}^{\frac{b}{2}} \frac{\Gamma_x\left(x_0 - x + U_0 - U\right) dx}{4\pi\left[\left(x_0 - x + U_0 - U\right)^2 + \left(W_0 - W\right)^2\right]} \tag{70}$$

The general lift circulation distribution is expressed as

$$\Gamma = \Gamma_r + \Gamma_e \tag{71}$$

where Γ_r and Γ_e are the rigid and elastic components of the lift circulation distribution which are given by

$$\Gamma_r = \frac{1}{2} V_\infty c c_{L_r} \tag{72}$$

$$\Gamma_e = \frac{1}{2} V_\infty c c_{L_\alpha}\left(-\frac{1 - \tan\alpha\Theta}{1 + \tan^2\alpha}\frac{\tan\alpha W_x^2}{2} - \Theta\right) \tag{73}$$

Therefore, the final expression for the total induced downwash is obtained as

$$w_i\left(x_0\right) = -\int_{-\frac{b}{2}}^{\frac{b}{2}} \frac{\left(\Gamma_{r,x} + \Gamma_{e,x}\right)\left(x_0 - x + U_0 - U\right) dx}{4\pi\left[\left(x_0 - x + U_0 - U\right)^2 + \left(W_0 - W\right)^2\right]} \tag{74}$$

Thus, the induced angle of attack is not only a function of the lift distribution but also is a function of the axial displacement, bending deflection, and torsional twist.

Consider a special case of the ideal elliptical lift distribution for which $\Gamma_r = \Gamma_0\sqrt{1 - \left(\frac{2x'}{b+2U_t}\right)^2}$ where $x' = x + U$ is the coordinate of the elastic axis for the deformed wing and $U_t = U\left(\frac{b}{2}\right)$. We use the coordinate of the deformed wing to specify lift distribution to ensure that the solution is physical. Otherwise, the lift circulation at $x' = \pm\frac{b}{2}$ does not exist since $x' \in \left[-\frac{b}{2} - U_t, \frac{b}{2} + U_t\right]$. Then, the downwash expression becomes

$$w_i\left(x_0\right) = -\int_{-\frac{b}{2}}^{\frac{b}{2}} \left[-\frac{4\Gamma_0 x'\left(1 + U_x\right)}{b^2\sqrt{1 - \left(\frac{2x'}{b+2U_t}\right)^2}} + \Gamma_{e,x}\right] \frac{\left(x_0 - x + U_0 - U\right) dx}{4\pi\left[\left(x_0 - x + U_0 - U\right)^2 + \left(W_0 - W\right)^2\right]} \tag{75}$$

For a rigid wing, the ideal elliptical lift distribution produces a uniform induced downwash and the minimum induced drag. The effect of the wing bending is to alter this uniform downwash for the ideal elliptical lift distribution. As a result, the ideal elliptical lift distribution may not yield the minimum induced drag due to the nonlinear large bending deflection.

B. Example

As an example, consider a constant-section high aspect ratio wing with 1-ft chord and 30-ft span. The cross section is a NACA 0012 with a wall thickness of 0.25 inches and a modulus of elasticity of 10×10^6 psi for aluminum. The cross sectional area and the flapwise area moment of inertia are computed to be $A = 2k_A c t_w$ and $I = \frac{4}{15}k_I c^3 t_w\left(\frac{t}{c}\right)^2$ where $k_A = 1.02032$ and $k_I = 1.03716$. The lift distribution is given by $l = 100\sqrt{1 - \left(\frac{2x}{b}\right)^2}$ lb/ft where $l = \rho_\infty V_\infty \Gamma$ for $\rho_\infty = 2.37756 \times 10^{-3}$ slug/ft^3 and $V_\infty = 300$ ft/sec corresponding to $M_\infty = 0.2687$. The lift curve slope is estimated from the formula $C_{L_\alpha} = \frac{2\pi}{\sqrt{1-M_\infty^2}+\frac{2}{\pi AR}}$ where $AR = 30$ is the aspect ratio. This yields $\alpha = 6.89°$. Figure 2 shows the linear and nonlinear deflections of the wing computed by applying the Galerkin method with 15 mode shapes to Eq. (66). Both the wing tip bending deflections as predicted by the linear and nonlinear bending theories are in close agreement The nonlinear bending theory yields a wing tip deflection of 3.0808 ft or 20.54% of the wing semi-span. In comparison, the linear bending theory predicts a wing tip deflection of 3.230 ft or 21.5% of the wing semi-span. Thus, the nonlinear bending theory predicts a smaller bending deflection than the linear bending theory. This difference is due primarily to the aeroelastic contribution of the last term in the left hand side of Eq. (66). The significant difference between the linear and nonlinear bending theories is the axial

displacement. For the linear bending theory, the axial displacement is exactly zero since there is no applied axial force. On the other hand, the nonlinear bending theory predicts an axial displacement of -0.3620 ft or -2.41% of the wing semi-span. As a result, the linear theory actually predicts an increase in the wing length by 2.6% of the wing semi-span, whereas the nonlinear theory preserves the length of the wing. This length-preserving property of the nonlinear bending theory in effect causes a reduction in the wing aspect ratio, which leads to an increase in the induced drag and decrease in lift as compared to the linear bending theory.

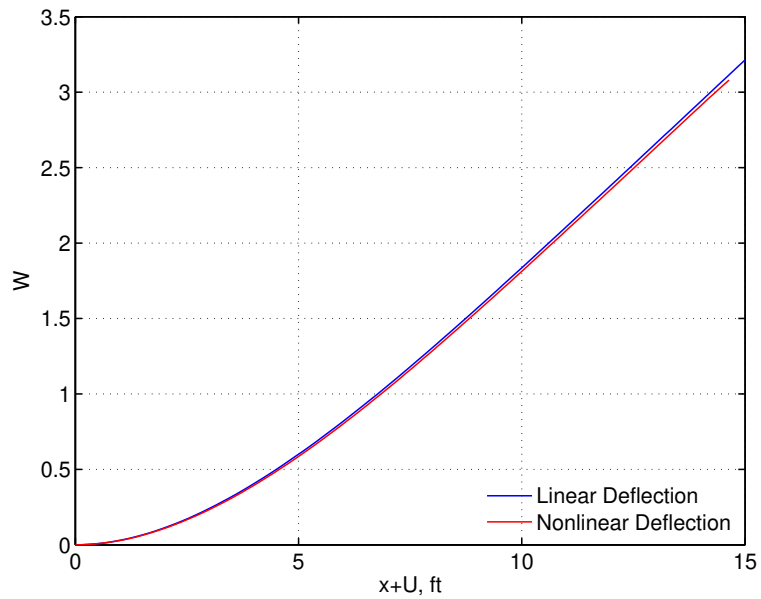

Figure 2. Linear and Nonlinear Bending Deflections

The length-preserving property of the nonlinear bending theory can be shown by examining Eq. (62) and ignoring the terms Θ_x^2 and W_{xx}^2. This leads to

$$U_x = \sqrt{1 - \left(\sin^{-1} W_x\right)^2} - 1 \approx -\frac{1}{2}\left(\sin^{-1} W_x\right)^2 \approx -\frac{1}{2} W_x^2 \tag{76}$$

The change in length due to the nonlinear bending deflection is computed as

$$\frac{ds}{dx} = \sqrt{\left(1 + U_x\right)^2 + W_x^2} = \sqrt{1 + \frac{W_x^4}{4}} \approx 1 \tag{77}$$

which shows the length-preserving property of the nonlinear bending theory.

For the linear bending theory, the increase in length is computed as

$$\Delta L = \int_0^L \left(\sqrt{1 + W_x^2} - 1\right) dx \approx \frac{1}{2}\int_0^L W_x^2 dx \tag{78}$$

Therefore, the linear bending theory yields a non-physical solution.

Also ignoring the term W_{xx}^2 in Eq. (66), the nonlinear static aeroelastic equation for bending can be approximated by the Taylor series of $\sin^{-1} W_x \approx W_x \left(1 + \frac{W_x^2}{6}\right)$. Then, the resulting equation is expressed as

$$\frac{\partial^2}{\partial x^2}\left[EI_{yy} W_{xx}\left(1 + \frac{W_x^4}{6}\right)\right] + c_{L_\alpha} q_\infty c \frac{\tan\alpha W_x^2}{2\left(1 + \tan^2\alpha\right)} = c_{L_r} q_\infty c - mg \tag{79}$$

Recognizing that $W_x^4 \approx 0$, then Eq. (79) becomes

$$\frac{\partial^2}{\partial x^2}\left(EI_{yy}W_{xx}\right) + c_{L_\alpha} q_\infty c \frac{\tan\alpha W_x^2}{2\left(1+\tan^2\alpha\right)} = c_{L_r} q_\infty c - mg \tag{80}$$

Thus, the difference in the bending deflection between the linear and nonlinear bending theories is due to mostly the aeroelastic term in the left hand side which contributes positively to the wing stiffness. For sweptback wings, truss-braced wings,[18] and rotary wings, the effect of the axial tension P_x can be a dominant factor. Then, the significance of the nonlinear bending deflection can be much more pronounced.

Figure 3 is the plot of the induced angle of attack $\alpha_i = \frac{w_i}{V_\infty}$ due to the induced downwash over the wing as computed by Eq. (75) which, for the constant chord and negligible torsional twist, is expressed as

$$w_i\left(x_0\right) = \int_{-\frac{b}{2}}^{\frac{b}{2}} \left(\frac{4\Gamma_0 x^{'}\left(1+U_x\right)}{b^2\sqrt{1-\left(\frac{2x'}{b+2U_t}\right)^2}} + \frac{1}{2}V_\infty c c_{L_\alpha}\frac{\tan\alpha W_x W_{xx}}{1+\tan^2\alpha} \right) \frac{\left(x_0 - x + U_0 - U\right)dx}{4\pi\left[\left(x_0 - x + U_0 - U\right)^2 + \left(W_0 - W\right)^2\right]} \tag{81}$$

Note that for the linear bending deflection, $\Gamma_{e,x} = 0$ and $U = 0$. So, the induced downwash is computed from the following equation:

$$w_i\left(x_0\right) = \int_{-\frac{b}{2}}^{\frac{b}{2}} \frac{\Gamma_0 x\left(x_0 - x\right)dx}{\pi b^2\sqrt{1-\left(\frac{2x}{b}\right)^2}\left[\left(x_0 - x\right)^2 + \left(W_0 - W\right)^2\right]} \tag{82}$$

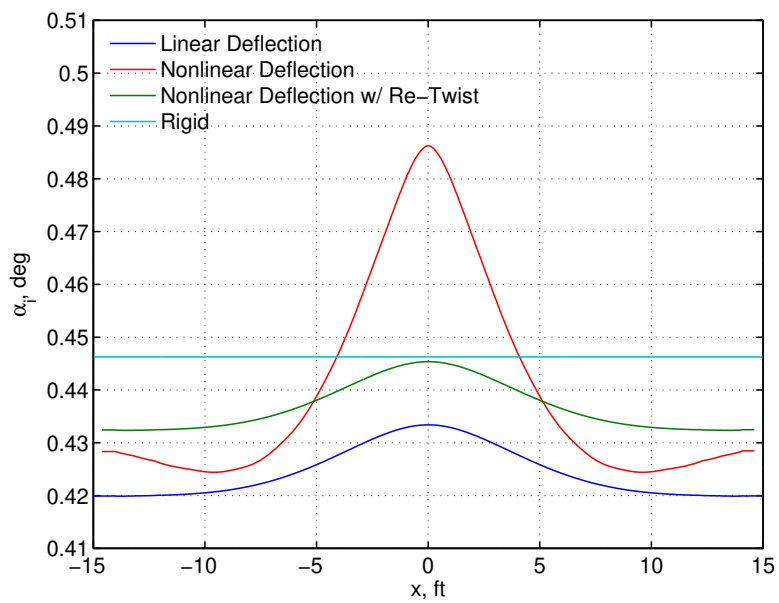

Figure 3. Induced Angles of Attack due to Bending Deflections

The rigid wing has a constant induced angle of attack for the ideal elliptical lift distribution whereas the bending deflection causes the induced angle of attack to become non-uniform with the maximum value at the mid-wing span. The linear deflection results in a lower induced angle of attack than the nonlinear deflection. This is due to the difference in the wing span where for the nonlinear deflection there is a reduction in the wing span which causes an increase in the induced downwash, hence induced angle of attack. The induced angle of attack at the center of the wing is the greatest with the nonlinear deflection. The results illustrate the significance of the effect of the nonlinear bending theory on the induced drag of a wing structure.

The lift coefficient is evaluated by taking into account of the wing bending deflection slope and the shortening of the wing span due to the axial displacement according to

$$C_L = \frac{1}{q_\infty S} \int_{-\frac{b}{2}}^{\frac{b}{2}} l\left(x^{'}\right) \cos\left(\sin^{-1} W_x\right)(1+U_x)\,dx = \frac{1}{q_\infty S} \int_{-\frac{b}{2}}^{\frac{b}{2}} l\left(x^{'}\right) \sqrt{1-W_x^2}\,(1+U_x)\,dx \tag{83}$$

where $l\left(x^{'}\right) == 100\sqrt{1-\left(\frac{2x^{'}}{b+2U_t}\right)^2}$.

The induced drag coefficient is evaluated from the following equation:

$$C_{D_i} = \frac{1}{q_\infty S} \int_{-\frac{b}{2}}^{\frac{b}{2}} l\left(x^{'}\right) \alpha_i\,(1+U_x)\,dx \tag{84}$$

Table 1 shows the lift and induced drag coefficients and the span efficiency factors ϵ based on the aspect ratio of the rigid wing for the linear deflection, nonlinear deflection, and rigid wing. The lift and drag coefficients are evaluated with the reduced wing span by $2U$ for the nonlinear bending deflection. It can be seen that the effect of the nonlinear bending deflection is to reduce the lift coefficient and increase the drag coefficient which results in a decrease in the span efficiency due to the change in the wing span. It is noted that the span efficiency factor can be greater than unity for non-planar wings as in the case with the linear bending deflection.

	C_L	C_{D_i}	ϵ
Linear Deflection	0.7166	0.005447	1.3958
Nonlinear Deflection	0.6846	0.005412	1.3422
Nonlinear Deflection with Re-Twist	0.6978	0.005450	1.3587
Rigid Wing	0.7338	0.005716	1

Table 1. Lift and Drag Coefficients and Span Efficiency Factors

C. Nonlinear Static Aeroelastic Analysis of a Flexible Swept Wing

A coupled aerodynamic-nonlinear finite element model is constructed for a sub-scale wind tunnel model of the Common Research Model (CRM)[19] to be tested in 2017 in the University of Washington Aeronautical Laboratory (UWAL) to validate a real-time adaptive drag optimization control strategy. This CRM model is designed to have about 10% wing tip deflection to represent the current state of the art high aspect ratio wings in modern transport aircraft such as the Boeing 777. The model is 85 inches in length with an elastic axis sweep angle of 31.5° and includes six active two-segment VCCTEF control surfaces as shown in Fig. 4. These surfaces are driven by actuators for the real-time drag minimization control strategy. The flow condition is at Mach 0.1162 and a dynamic pressure of 20 psf. The aerodynamic model is a wind tunnel sub-scale model of a CRM wing to be tested in the UWAL in 2018 to demonstrate an active real-time drag optimization control strategy.

The model is developed within a multidisciplinary coupled aerodynamic-nonlinear finite element analysis framework as shown in Fig. 5. The framework consists of four computational modules: 1) NASA vortex-lattice code VORLAX[20] developed by Louis Miranda et al. with a pre-processor VORVIEW for providing a graphical user interface (GUI) for model geometry handling, 2) 2D Euler CFD code MSES with an integral boundary layer method developed by Mark Drela,[21] 3) an in-house computational geometry code that manipulates the model geometry deformation, and 4) an in-house nonlinear 3D beam finite-element analysis (FEA) code with structural dynamics and aeroelasticity capabilities. The framework can compute the solution for a specified lift coefficient input or angle of attack input. For each solution for lift matching, VORLAX iteratively computes the angle of attack to match the specified lift coefficient. Then, the solution is corrected for the viscous and, if necessary, transonic flow effect with MSES which computes the lift and drag coefficients for each wing station in the VORLAX model. This transonic and viscous correction method requires an iteration loop between MSES and VORLAX. Once the corrections are made, VORLAX determines the new

angle of attack iteratively to match the specified lift coefficient. At this point, the aerodynamic forces and moments are computed and then passed to the FEA code. The FEA code computes the wing deflections and then passes this deflection information to the computational geometry module which computes the geometry of the model deformation. This updated geometry is then passed to VORVIEW for geometry processing. The solution process is then repeated until the angle of attack converges to within a specified tolerance.

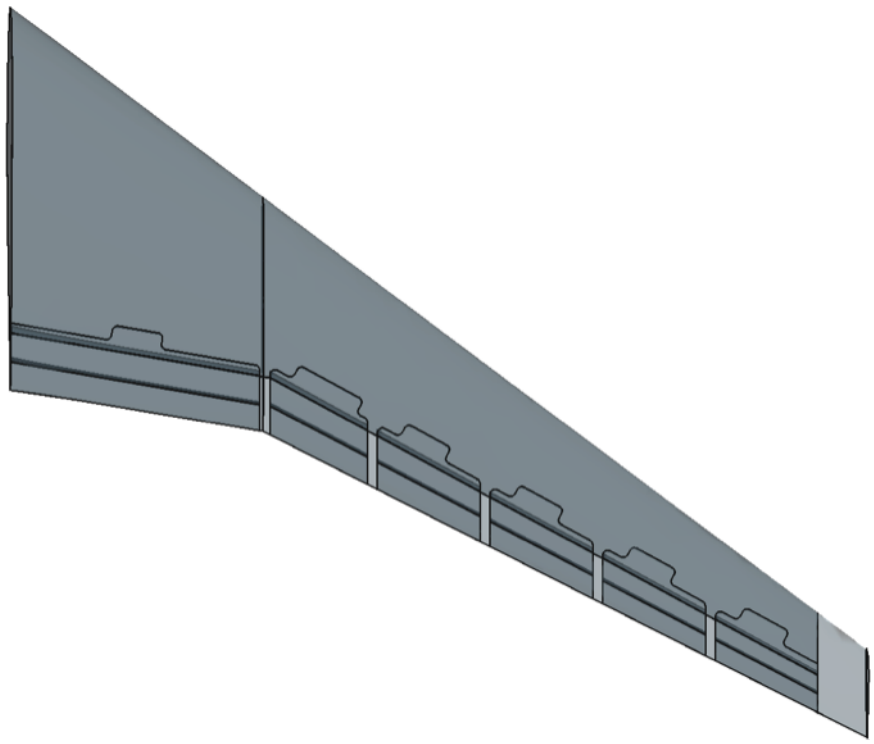

Figure 4. Common Research Model Sub-Scale Wind Tunnel Model in UWAL

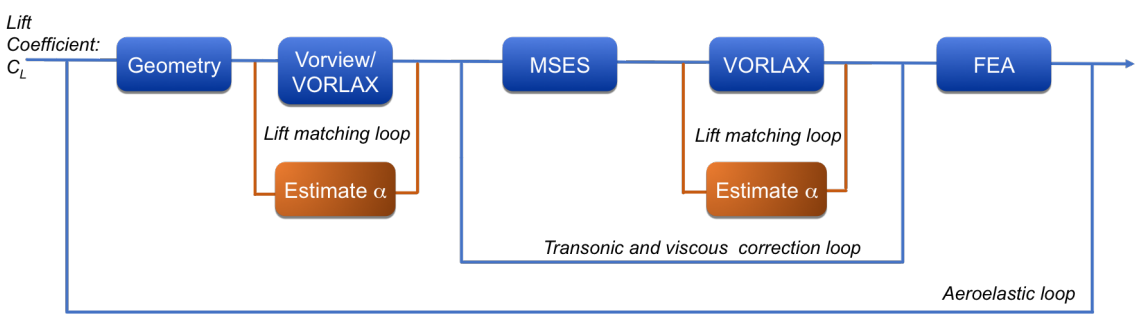

Figure 5. Coupled Aerodynamic-Nonlinear Finite Element Analysis Framework

The displacement matrix equation is nonlinear and can be solved for the static aeroelastic deflections by any nonlinear root search methods. One iterative method is proposed as follows:

- For $i = 0$, initialize $U_i(x) = 0$, $V_i(x) = 0$, $W_i(x) = 0$, and $\Theta_i(x) = 0$. Evaluate $\mathbf{K}_i$. Then, compute

$$\mathbf{x}_i = \mathbf{K}_i^{-1}\mathbf{F} \tag{85}$$

- For $i = 1, 2, \ldots, n$, evaluate $U_i(x)$, $V_i(x)$, $W_i(x)$, and $\Theta_i(x)$. Update $\mathbf{K}_i$. Then, iterate

$$\mathbf{x}_i = m\mathbf{x}_{i-1} + (1-m)\,\mathbf{K}_i^{-1}\mathbf{F} \tag{86}$$

  with $0 \leq m < 1$ until $\mathbf{x}_i$ converges. Note that this algorithm will ensure numerical stability and converge to the 'exact' solution of Eq. (85) in the limit as $n \to \infty$. Equation (86) essentially imposes the stability condition on the unit circle. Otherwise, if Eq. (85) is used instead which corresponds to $m = 0$, numerical stability issues sometimes may be encountered. A suitable value for m is usually in the range between $\frac{1}{3}$ and $\frac{1}{2}$.

Figure 6 shows the convergence of the iterative nonlinear solution according to Eq. (86) for three values of $m = 0, \frac{1}{3}, \frac{1}{2}$. The wing tip deflection W_t at the angle of attack of 7.616° is plotted as a function of the iteration number. The results show that the solution converges the fastest with $m = 0$ after only two iterations. As m increases, the convergence is slower. It is noted that in other situations where the nonlinear effects are much more dominant, experiences support the use of a positive value for m between $\frac{1}{3}$ and $\frac{1}{2}$.

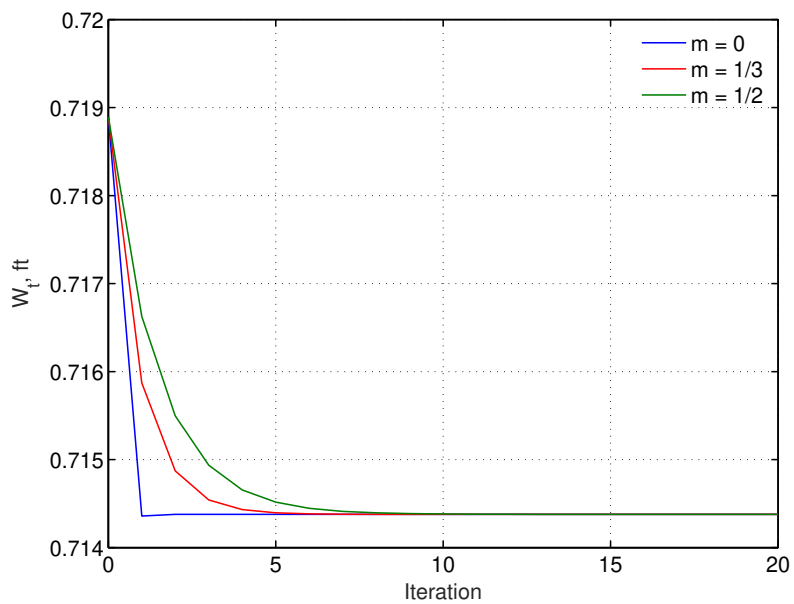

Figure 6. CRM Sub-Scale Model Solution Convergence at $\alpha = 7.616°$

Figure 7 shows the linear and nonlinear bending deflections of the CRM sub-scale model along the aircraft pitch axis y computed for the angle of attack of 9.538°. The linear deflection at the wing tip is 10.17 inches versus the nonlinear deflection of 10.11 inches. The wing length measured along the elastic axis is 99.69 inches. So the wing tip deflection is 10% of the wing length. The nonlinear deflection is only slightly smaller than but essentially the same as the linear deflection.

Figure 8 shows the linear and nonlinear axial displacements of the CRM sub-scale model along the aircraft pitch axis y. The linear theory predicts an axial displacement of 0.01456 inches at the wing tip whereas the nonlinear theory predicts an axial displacement of -0.7124 inches. The axial extension with the linear theory is due to the drag force component along the swept elastic axis. As expected, the axial displacement computed by the linear theory is non-physical since it predicts a larger elongation of the wing than is possible. The linear theory predicts an elongation of 0.8396 inches as compared to the nonlinear theory which predicts an elongation of only 0.1136 inches due to the drag component along the elastic axis.

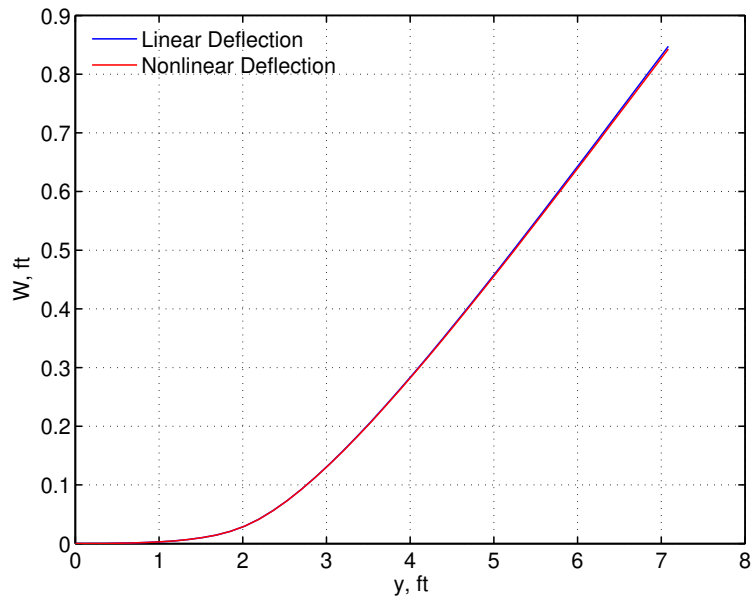

Figure 7. CRM Sub-Scale Model Flapwise Bending Deflection at $\alpha = 9.538°$

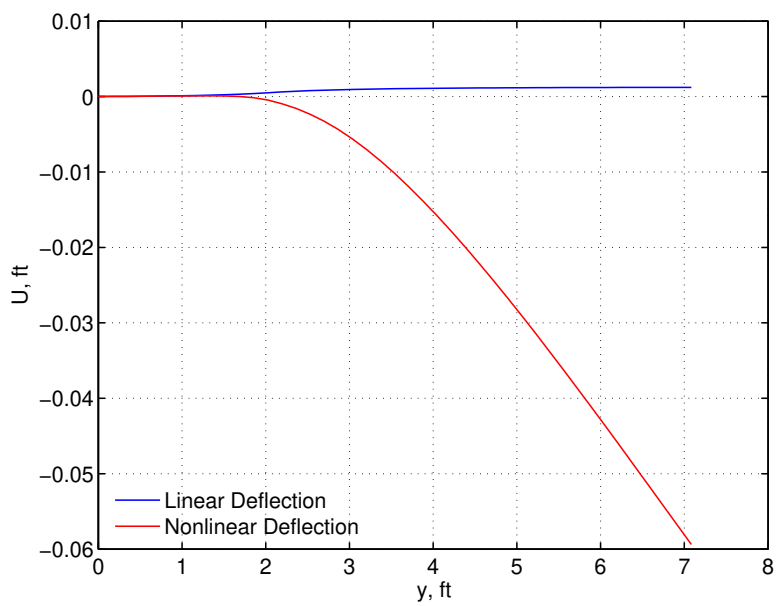

Figure 8. CRM Sub-Scale Model Axial Displacement at $\alpha = 9.538°$

Figure 9 shows the linear and nonlinear chordwise bending deflections of the CRM sub-scale model along the aircraft pitch axis y. As expected, the chordwise bending deflections are very small due to the much larger chordwise bending stiffness and the small drag force component acting normal to the elastic axis. Nonetheless, the difference between the linear and nonlinear bending theories is revealing. The nonlinear

bending theory predicts a larger chordwise bending deflection but in the opposite direction than the linear bending theory. This is due to the contribution of the nonlinear term $\sin^{-1} W_x \Theta_x$ in Eq. (31) which causes a negative contribution to the chordwise bending deflection.

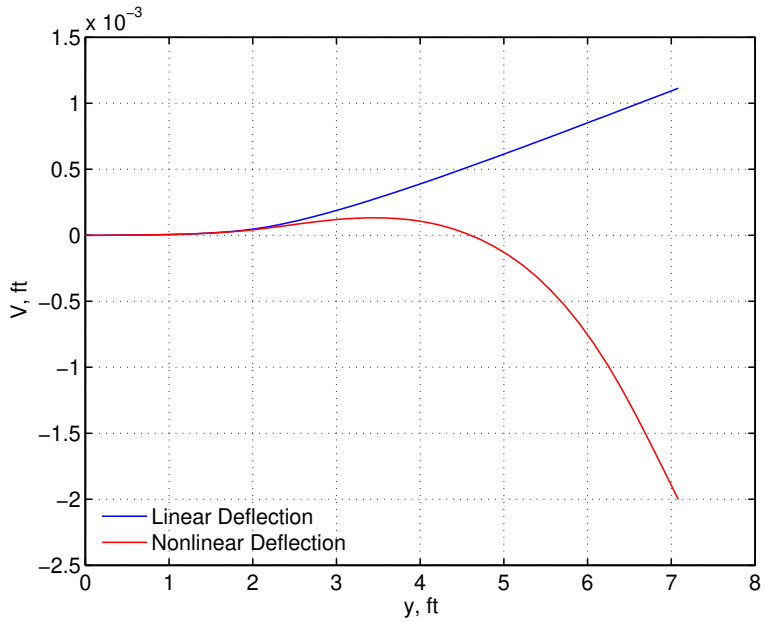

Figure 9. CRM Sub-Scale Model Chordwise Bending Deflection at $\alpha = 9.538°$

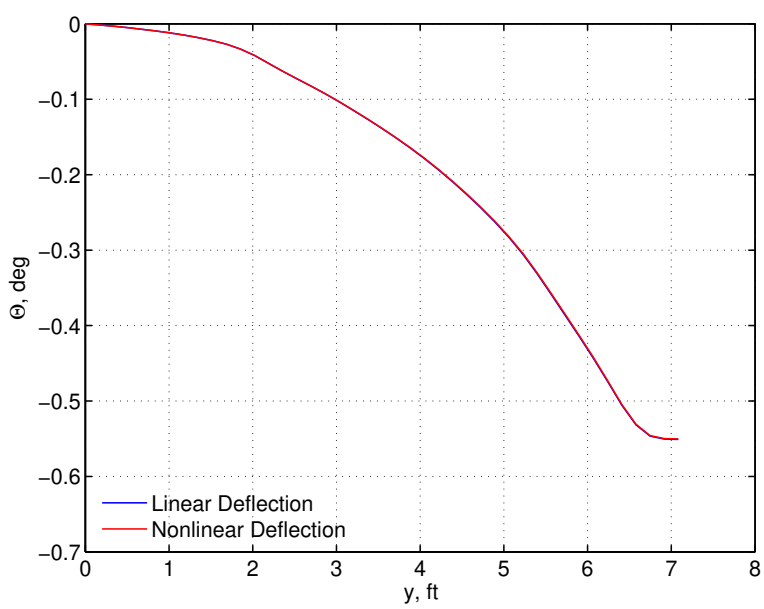

Figure 10. CRM Sub-Scale Model Torsional Twist at $\alpha = 9.538°$

Figure 10 shows the linear and nonlinear torsional twists of the CRM sub-scale model along the aircraft pitch axis y. Both the linear and nonlinear torsional twists are virtually the same. The nonlinear theory predicts a smaller torsional twist than the linear theory due to the presence of the small axial tension caused by the drag component along the elastic axis which acts to increase the torsional stiffness. This is observed in the results which show that the nonlinear torsional twist at the wing tip of $-0.5502°$ is slightly smaller than the linear torsional twist of $-0.5510°$.

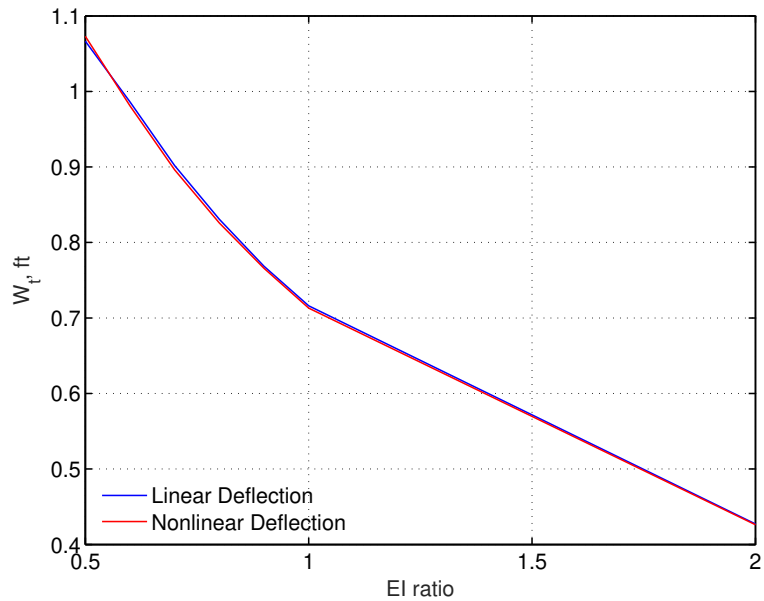

Figure 11. CRM Sub-Scale Model Flapwise Bending Deflection vs. Bending Stiffness

Figure 11 shows the effect of the flapwise bending stiffness on the linear and nonlinear bending deflections at the wing tip. The nonlinear bending deflection is generally smaller than the linear bending deflection, but as the stiffness is reduced by 50%, the trend is reverse. As the stiffness increases, the nonlinear and linear bending deflections appear to converge. This is expected because as the stiffness increases the bending deflection decreases until it is small enough that the linear bending theory holds.

Figure 12 shows the lift curves of the CRM sub-scale model. The rigid wing produces more lift at a given angle of attack than the flexible wing as expected. Both the linear and nonlinear bending deflections give almost the same lift curves. On a closer look, the lift curve for the linear bending deflection is slightly higher than that for the nonlinear bending deflection. This becomes more apparent in Fig. 13. As the wing becomes stiffer, the difference in the lift coefficient between the nonlinear and linear bending deflection decreases.

Figure 14 shows the drag polar of the CRM sub-scale model. For the wind tunnel test, a jig shape twist optimization has been conducted to determine the optimal jig-shape twist that minimizes the induced drag for the CRM sub-scale model in its deflected state in the wind tunnel. As a result, at a fixed value of the lift coefficient, the rigid wing produces a higher drag than the flexible wing. The linear and nonlinear bending deflections both produce nearly identical drag coefficients. On a closer look, the drag coefficient for the nonlinear bending deflection appears to be slightly smaller than that for the linear bending deflection but not by much. At the angle of attack of 8°, the drag coefficients for the linear and nonlinear deflections are 0.020560 and 0.020557, respectively. Figure 15 which shows that the drag coefficient for the nonlinear bending deflection is lower than that for the linear bending deflection as the wing bending stiffness varies.

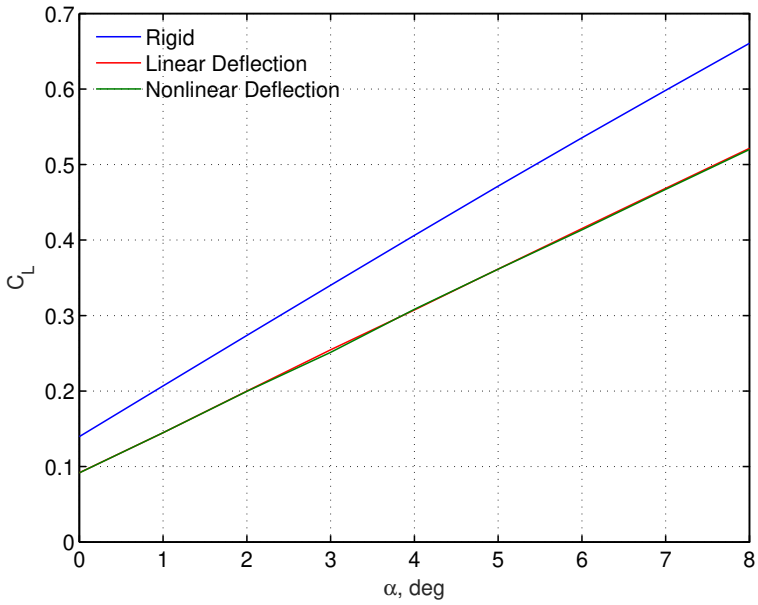

Figure 12. CRM Sub-Scale Drag Model Lift Coefficient vs. Angle of Attack at $M_\infty = 0.1162$

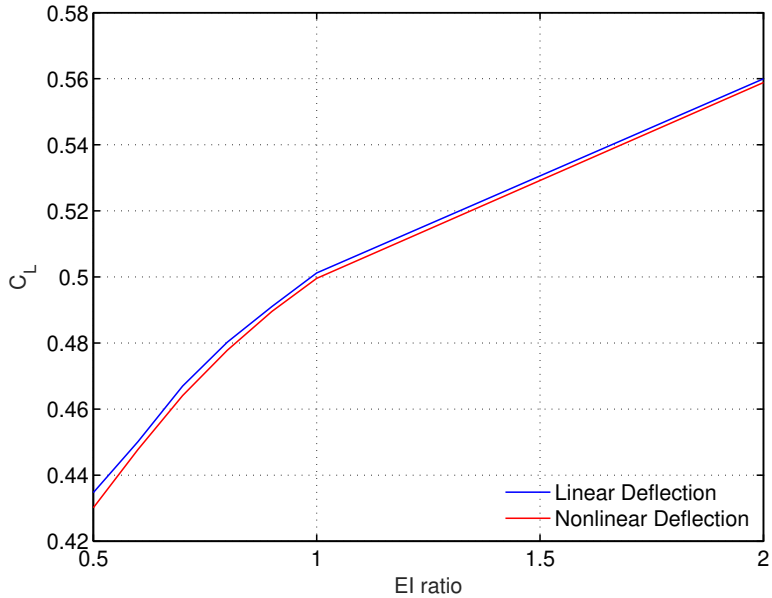

Figure 13. CRM Sub-Scale Drag Model Lift Coefficient at $\alpha = 7.616°$ and $M_\infty = 0.1162$ vs. Bending Stiffness

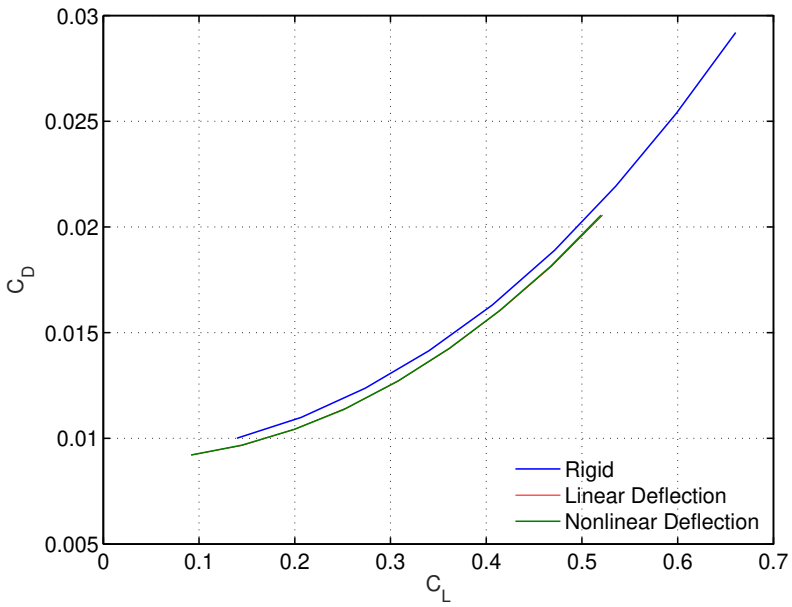

Figure 14. CRM Sub-Scale Model Drag Polar

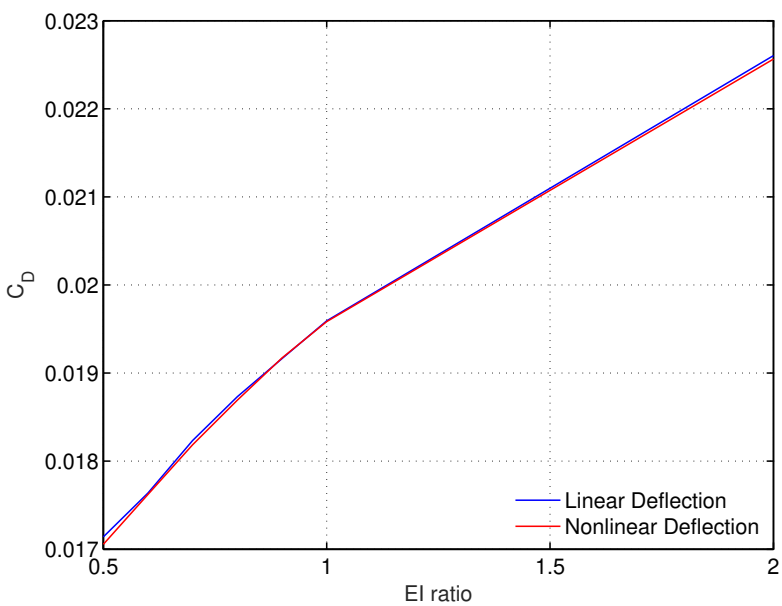

Figure 15. CRM Sub-Scale Model Drag Polar

VI. Nonlinear Effect of Limit Cycle Oscillations

Consider the case of static aeroelasticity of unswept wings for which $f_x = 0$. Neglecting the axial displacement and chordwise bending contributions and making the assumption that $\tan\alpha\Theta \approx 0$ and $\tan^2\alpha \approx$

0, the aeroelastic angle of attack is expressed as

$$\alpha_e(y) = -\frac{\tan\alpha W_x^2}{2} - \frac{y\left(1-\frac{W_x^2}{2}\right)\Theta_t}{V_\infty} - \Theta - \frac{\left(1-\frac{W_x^2}{2}\right)W_t}{V_\infty} \tag{87}$$

The non-circulatory lift and pitching moment coefficients are then obtained as

$$c_{L_{nc}} = \frac{\pi c}{2V_\infty}\left[-\tan\alpha W_x W_{xt} - \frac{e_m\left(1-W_xW_{xt}\right)\Theta_t}{V_\infty} - \frac{e_m\left(1-\frac{W_x^2}{2}\right)\Theta_{tt}}{V_\infty} - \Theta_t + \frac{W_xW_{xt}W_t}{V_\infty} - \frac{\left(1-\frac{W_x^2}{2}\right)W_{tt}}{V_\infty}\right] \approx \frac{\pi c}{2V_\infty}\left[-\tan\alpha W_x W_{xt} - \frac{e_m\left(1-\frac{W_x^2}{2}\right)\Theta_{tt}}{V_\infty} - \Theta_t - \frac{\left(1-\frac{W_x^2}{2}\right)W_{tt}}{V_\infty}\right] \tag{88}$$

$$c_{m_{nc}} = \frac{\pi c}{8}\frac{\left(1-\frac{W_x^2}{2}\right)\Theta_t}{V_\infty} + \frac{\pi c^2}{64V_\infty}\frac{\left(1-\frac{W_x^2}{2}\right)\Theta_{tt}}{V_\infty} + \frac{\pi e_m}{2V_\infty}\left[\tan\alpha W_x W_{xt} + \frac{e_m\left(1-\frac{W_x^2}{2}\right)\Theta_{tt}}{V_\infty} + \Theta_t + \frac{\left(1-\frac{W_x^2}{2}\right)W_{tt}}{V_\infty}\right] = \frac{\pi}{2V_\infty}\left[e_m\tan\alpha W_x W_{xt} + \frac{\left(c^2+32e_m^2\right)\left(1-\frac{W_x^2}{2}\right)\Theta_{tt}}{32V_\infty} + \left(e_c - \frac{cW_x^2}{8}\right)\Theta_t + \frac{e_m\left(1-\frac{W_x^2}{2}\right)W_{tt}}{V_\infty}\right] \tag{89}$$

The dynamics of the axial displacement are usually associated with higher frequencies than the dynamics of the bending and torsion. Instead, U_x is given by Eq. (76) and note that $\frac{1+U_x}{\sqrt{1-W_x^2}} \approx 1$. The dynamic aeroelastic equations are then obtained as

$$\frac{\partial^2}{\partial x^2}\left(EI_{yy}W_{xx}\right) = -\rho A\left(W_{tt} + e_{cg}\Theta_{tt}\right) + \frac{\partial}{\partial x}\left(\rho I_{yy}\frac{W_{xtt}}{\sqrt{1-W_x^2}}\right) + l_r - \rho A g + q_\infty cC(k)\,c_{L_\alpha}\left[-\frac{\tan\alpha W_x^2}{2} - \frac{e_c\left(1-\frac{W_x^2}{2}\right)\Theta_t}{V_\infty} - \Theta - \frac{\left(1-\frac{W_x^2}{2}\right)W_t}{V_\infty}\right] + q_\infty\frac{\pi c^2}{2V_\infty}\left[-\tan\alpha W_x W_{xt} - \frac{e_m\left(1-\frac{W_x^2}{2}\right)\Theta_{tt}}{V_\infty} - \Theta_t - \frac{\left(1-\frac{W_x^2}{2}\right)W_{tt}}{V_\infty}\right] \tag{90}$$

$$\frac{\partial}{\partial x}\left(GJ\Theta_x\right) = \rho A e_{cg}W_{tt} + \rho I_{xx}\Theta_{tt} + m_r - \rho A g e_{cg} + q_\infty ceC(k)\,c_{L_\alpha}\left[-\frac{\tan\alpha W_x^2}{2} - \frac{e_c\left(1-\frac{W_x^2}{2}\right)\Theta_t}{V_\infty} - \Theta - \frac{\left(1-\frac{W_x^2}{2}\right)W_t}{V_\infty}\right] + q_\infty\frac{\pi c^2}{2V_\infty}\left[e_m\tan\alpha W_x W_{xt} + \frac{\left(c^2+32e_m^2\right)\left(1-\frac{W_x^2}{2}\right)\Theta_{tt}}{32V_\infty} + \left(e_c - \frac{cW_x^2}{8}\right)\Theta_t + \frac{e_m\left(1-\frac{W_x^2}{2}\right)W_{tt}}{V_\infty}\right] \tag{91}$$

A. Weak-Form Aeroelastic Equations

The nonlinear partial differential equations are usually referred to as a strong form. A numerical solution can be performed by converting the strong-form partial differential equations into weak-form differential

equations by letting $U(x,t) = \mathbf{N}_u(x)\,\mathbf{u}(t)$, $W(x,t) = \mathbf{N}_w(x)\,\mathbf{w}(t)$, and $\Theta(x,t) = \mathbf{N}_\theta(x)\,\boldsymbol{\theta}(t)$. For the Galerkin method, $\mathbf{N}_u(x)$, $\mathbf{N}_v(x)$, $\mathbf{N}_w(x)$, and$\mathbf{N}_\theta(x)$ are the vectors of the mode shapes over the domain of the solution $x \in [0, L]$, whereas for the finite element method they are the vectors of interpolation functions over the domain of the solution for an element $x \in [0, l]$. The vectors $\mathbf{u}(t)$, $\mathbf{w}(t)$, and $\boldsymbol{\theta}(t)$ represent the generalized coordinates in the Galerkin method, or the nodal displacements including the bending slopes in the finite element method.

We use the Taylor series expansion of $\frac{1}{\sqrt{1-W_x^2}} \approx 1 + \frac{W_x^2}{2}$. Then, pre-multiplying Eqs. (28) to (31) by $\mathbf{N}_u^\top(x)$, $\mathbf{N}_v^\top(x)$, $\mathbf{N}_w^\top(x)$, and $\mathbf{N}_\theta^\top(x)$, respectively, and integrating over the domain of the solution yield

$$\begin{aligned}\int \left(\mathbf{N}_w''^\top EI_{yy}\mathbf{N}_w''\right)\mathbf{w}dx = &-\int \mathbf{N}_w^\top \rho A\left(\mathbf{N}_w\ddot{\mathbf{w}} + e_{cg}\mathbf{N}_\theta\ddot{\boldsymbol{\theta}}\right)dx - \int \mathbf{N}_w'^\top \rho I_{yy}\left(1+\frac{W_x^2}{2}\right)\mathbf{N}_w'\ddot{\mathbf{w}} \\ &+ \int \mathbf{N}_w^\top(l_r - \rho Ag)\,dx + q_\infty \int \mathbf{N}_w^\top cC(k)\,c_{L_\alpha}\left[-\frac{\tan\alpha W_x}{2}\mathbf{N}_w'\mathbf{w} - \frac{e_c\left(1-\frac{W_x^2}{2}\right)}{V_\infty}\mathbf{N}_\theta\dot{\boldsymbol{\theta}} - \mathbf{N}_\theta\boldsymbol{\theta}\right. \\ &\left. -\frac{\left(1-\frac{W_x^2}{2}\right)}{V_\infty}\mathbf{N}_w\dot{\mathbf{w}}\right]dx + q_\infty\int \mathbf{N}_w^\top\frac{\pi c^2}{2V_\infty}\left[-\tan\alpha W_x\mathbf{N}_w'\dot{\mathbf{w}} - \frac{e_m\left(1-\frac{W_x^2}{2}\right)}{V_\infty}\mathbf{N}_\theta\ddot{\boldsymbol{\theta}} - \mathbf{N}_\theta\dot{\boldsymbol{\theta}}\right. \\ &\left. -\frac{\left(1-\frac{W_x^2}{2}\right)}{V_\infty}\mathbf{N}_w\ddot{\mathbf{w}}\right]dx \end{aligned} \tag{92}$$

$$\begin{aligned}-\int \mathbf{N}_\theta'^\top GJ\mathbf{N}_\theta'\boldsymbol{\theta}dx = &\int \mathbf{N}_\theta^\top \rho Ae_{cg}\mathbf{N}_w\ddot{\mathbf{w}}dx + \int \mathbf{N}_\theta^\top \rho I_{xx}\mathbf{N}_\theta\ddot{\boldsymbol{\theta}}dx + \int \mathbf{N}_\theta^\top(m_r - \rho Age_{cg})\,dx \\ &+ q_\infty\int \mathbf{N}_\theta^\top ceC(k)\,c_{L_\alpha}\left[-\frac{\tan\alpha W_x}{2}\mathbf{N}_w'\mathbf{w} - \frac{e_c\left(1-\frac{W_x^2}{2}\right)}{V_\infty}\mathbf{N}_\theta\dot{\boldsymbol{\theta}} - \mathbf{N}_\theta\boldsymbol{\theta} - \frac{\left(1-\frac{W_x^2}{2}\right)}{V_\infty}\mathbf{N}_w\dot{\mathbf{w}}\right]dx \\ &+ q_\infty\int \mathbf{N}_\theta^\top\frac{\pi c^2}{2V_\infty}\left[e_m\tan\alpha W_x\mathbf{N}_w'\dot{\mathbf{w}} + \frac{\left(c^2+32e_m^2\right)\left(1-\frac{W_x^2}{2}\right)}{32V_\infty}\mathbf{N}_\theta\ddot{\boldsymbol{\theta}} + \left(e_c - \frac{cW_x^2}{8}\right)\mathbf{N}_\theta\dot{\boldsymbol{\theta}}\right. \\ &\left. + \frac{e_m\left(1-\frac{W_x^2}{2}\right)}{V_\infty}\mathbf{N}_w\ddot{\mathbf{w}}\right]dx \end{aligned} \tag{93}$$

The problem is cast as

$$\mathbf{M}(W_x)\,\ddot{\mathbf{x}} + \mathbf{C}(W_x)\,\dot{\mathbf{x}} + \mathbf{K}(W_x)\,\mathbf{x} = \mathbf{F} \tag{94}$$

where $\mathbf{x} = \begin{bmatrix}\mathbf{w}^\top & \boldsymbol{\theta}^\top\end{bmatrix}^\top$; $\mathbf{M}$, $\mathbf{C}$, and $\mathbf{K}$ are the nonlinear mass, damping, and stiffness matrices, respectively; and $\mathbf{F}$ is the force vector. The nonlinear global stiffness matrix and force vector are assembled from the following elemental stiffness matrix and force vector:

$$\mathbf{m} = \begin{bmatrix}\mathbf{m}_{ww} & \mathbf{m}_{w\theta} \\ \mathbf{m}_{\theta w} & \mathbf{k}_{\theta\theta}\end{bmatrix} \tag{95}$$

$$\mathbf{c} = \begin{bmatrix}\mathbf{c}_{ww} & \mathbf{c}_{w\theta} \\ \mathbf{c}_{\theta w} & \mathbf{k}_{\theta\theta}\end{bmatrix} \tag{96}$$

$$\mathbf{k} = \begin{bmatrix}\mathbf{k}_{ww} & \mathbf{k}_{w\theta} \\ \mathbf{k}_{\theta w} & \mathbf{k}_{\theta\theta}\end{bmatrix} \tag{97}$$

$$\mathbf{f} = \int \begin{bmatrix}\mathbf{N}_w^\top(l_r - \rho Ag) \\ -\mathbf{N}_\theta^\top(m_r - \rho Age_{cg})\end{bmatrix}dx \tag{98}$$

where

$$\mathbf{m}_{ww} = \int \left\{ \left[\rho A + \frac{q_\infty \pi c^2 \left(1 - \frac{W_x^2}{2}\right)}{2V_\infty^2} \right] \mathbf{N}_w^\top \mathbf{N}_w + \rho I_{yy} \left(1 + \frac{W_x^2}{2}\right) \mathbf{N}_w'^\top \mathbf{N}_w' \right\} dx \tag{99}$$

$$\mathbf{m}_{w\theta} = \int \left[\rho A e_{cg} + \frac{q_\infty \pi c^2 e_m \left(1 - \frac{W_x^2}{2}\right)}{2V_\infty^2} \right] \mathbf{N}_w^\top \mathbf{N}_\theta dx \tag{100}$$

$$\mathbf{m}_{\theta w} = \int \left[\rho A e_{cg} + \frac{q_\infty \pi c^2 e_m \left(1 - \frac{W_x^2}{2}\right)}{2V_\infty^2} \right] \mathbf{N}_\theta^\top \mathbf{N}_w dx \tag{101}$$

$$\mathbf{m}_{\theta\theta} = \int \left[\rho I_{xx} + \frac{q_\infty \pi c^2 \left(c^2 + 32 e_m^2\right) \left(1 - \frac{W_x^2}{2}\right)}{64V_\infty^2} \right] \mathbf{N}_\theta^\top \mathbf{N}_\theta dx \tag{102}$$

$$\mathbf{c}_{ww} = \int \frac{q_\infty c}{V_\infty} \left[C(k)\, c_{L_\alpha} \left(1 - \frac{W_x^2}{2}\right) \mathbf{N}_w^\top \mathbf{N}_w + \frac{\pi c \tan \alpha W_x}{2} \mathbf{N}_w^\top \mathbf{N}_w' \right] dx \tag{103}$$

$$\mathbf{c}_{w\theta} = \int \frac{q_\infty c}{V_\infty} \left[C(k)\, c_{L_\alpha} e_c \left(1 - \frac{W_x^2}{2}\right) + \frac{\pi c}{2} \right] \mathbf{N}_w^\top \mathbf{N}_\theta dx \tag{104}$$

$$\mathbf{c}_{\theta w} = \int \frac{q_\infty c}{V_\infty} \left[-eC(k)\, c_{L_\alpha} \left(1 - \frac{W_x^2}{2}\right) \mathbf{N}_\theta^\top \mathbf{N}_w + \frac{\pi c e_m \tan \alpha W_x}{2} \mathbf{N}_\theta^\top \mathbf{N}_w' \right] dx \tag{105}$$

$$\mathbf{c}_{\theta\theta} = \int \frac{q_\infty c}{V_\infty} \left[-eC(k)\, c_{L_\alpha} e_c \left(1 - \frac{W_x^2}{2}\right) + \frac{\pi c \left(e_c - \frac{c W_x^2}{8}\right)}{2} \right] \mathbf{N}_\theta^\top \mathbf{N}_\theta dx \tag{106}$$

$$\mathbf{k}_{ww} = \int \left[EI_{yy} \mathbf{N}_w''^\top \mathbf{N}_w'' + \frac{q_\infty c C(k)\, c_{L_\alpha} \tan \alpha W_x}{2} \mathbf{N}_w^\top \mathbf{N}_w' \right] dx \tag{107}$$

$$\mathbf{k}_{w\theta} = \int q_\infty c C(k)\, c_{L_\alpha} \mathbf{N}_w^\top \mathbf{N}_\theta dx \tag{108}$$

$$\mathbf{k}_{\theta w} = -\int \frac{q_\infty c e C(k)\, c_{L_\alpha} \tan \alpha W_x}{2} \mathbf{N}_\theta^\top \mathbf{N}_w' dx \tag{109}$$

$$\mathbf{k}_{\theta\theta} = \int \left[GJ \mathbf{N}_\theta'^\top \mathbf{N}_\theta' - q_\infty c e C(k)\, c_{L_\alpha} \mathbf{N}_\theta^\top \mathbf{N}_\theta \right] dx \tag{110}$$

Equation (94) is a complex-valued equation due to the Theodorsen's complex-valued function $C(k)$. It can be expressed as follows:

$$\mathbf{M}\ddot{\mathbf{x}} + \left[\mathbf{C}_0 + \mathbf{C}_1 C(k)\right] \dot{\mathbf{x}} + \left[\mathbf{K}_0 + \mathbf{K}_1 C(k)\right] \mathbf{x} = \mathbf{F} \tag{111}$$

The Theodorsen's function can be approximated by the R. T. Jones' approximation method as follows:

$$C(k)\,\mathbf{x} \approx \hat{C}(\bar{s})\,\mathbf{x} = \frac{0.5\bar{s}^2 + a_1\bar{s} + a_2}{\bar{s}^2 + a_3\bar{s} + a_2}\mathbf{x} = 0.5\mathbf{x} + \frac{a_4\bar{s} + 0.5a_2}{\bar{s}^2 + a_3\bar{s} + a_2}\mathbf{x} \tag{112}$$

$$C(k)\,\dot{\mathbf{x}} \approx \hat{C}(\bar{s})\, s\mathbf{x} = \frac{0.5\bar{s}^3 + a_1\bar{s}^2 + a_2\bar{s}}{\bar{s}^2 + a_3\bar{s} + a_2} \left(\frac{2V_\infty}{c}\right) \mathbf{x} = 0.5s\mathbf{x} + a_4 \left(\frac{2V_\infty}{c}\right) \mathbf{x} + \frac{a_5\bar{s} + a_6}{\bar{s}^2 + a_3\bar{s} + a_2} \left(\frac{2V_\infty}{c}\right) \mathbf{x} \tag{113}$$

where $\bar{s} = \frac{sc}{2V_\infty}$, $a_1 = 0.2808$, $a_2 = 0.01365$, $a_3 = 0.3455$, and

$$a_4 = a_1 - 0.5a_3 \tag{114}$$

$$a_5 = 0.5a_2 - a_1a_3 + 0.5a_3^2 \tag{115}$$

$$a_6 = -a_1a_2 + 0.5a_2a_3 \tag{116}$$

Let

$$\mathbf{y} = \frac{a_4\bar{s} + 0.5a_2}{\bar{s}^2 + a_3\bar{s} + a_2}\mathbf{x} \tag{117}$$

$$\mathbf{z} = \frac{a_5\bar{s} + a_6}{\bar{s}^2 + a_3\bar{s} + a_2}\mathbf{x} \tag{118}$$

Then,

$$\ddot{\mathbf{y}} + a_3\left(\frac{2V_\infty}{c}\right)\dot{\mathbf{y}} + a_2\left(\frac{2V_\infty}{c}\right)^2\mathbf{y} = a_4\left(\frac{2V_\infty}{c}\right)\dot{\mathbf{x}} + 0.5a_2\left(\frac{2V_\infty}{c}\right)^2\mathbf{x} \tag{119}$$

$$\ddot{\mathbf{z}} + a_3\left(\frac{2V_\infty}{c}\right)\dot{\mathbf{z}} + a_2\left(\frac{2V_\infty}{c}\right)^2\mathbf{z} = a_5\left(\frac{2V_\infty}{c}\right)\dot{\mathbf{x}} + a_6\left(\frac{2V_\infty}{c}\right)^2\mathbf{x} \tag{120}$$

Equation (94) becomes

$$\mathbf{M}\ddot{\mathbf{x}} + (\mathbf{C}_0 + 0.5\mathbf{C}_1)\dot{\mathbf{x}} + \left[\mathbf{K}_0 + 0.5\mathbf{K}_1 + a_4\left(\frac{2V_\infty}{c}\right)\mathbf{C}_1\right]\mathbf{x} + \mathbf{K}_1\mathbf{y} + \left(\frac{2V_\infty}{c}\right)\mathbf{C}_1\mathbf{z} = \mathbf{F} \tag{121}$$

The combined system of equations is now defined as

$$\mathbf{M}_a\ddot{\mathbf{x}}_a + \mathbf{C}_a\dot{\mathbf{x}}_a + \mathbf{K}_a\mathbf{x}_a = \mathbf{F}_a \tag{122}$$

where $\mathbf{x}_a = \begin{bmatrix} \mathbf{x}^\top & \mathbf{y}^\top & \mathbf{z}^\top \end{bmatrix}^\top$ and

$$\mathbf{M}_a = \begin{bmatrix} \mathbf{M} & \mathbf{0} & \mathbf{0} \\ \mathbf{0} & \mathbf{I} & \mathbf{0} \\ \mathbf{0} & \mathbf{0} & \mathbf{I} \end{bmatrix} \tag{123}$$

$$\mathbf{C}_a = \begin{bmatrix} \mathbf{C}_0 + 0.5\mathbf{C}_1 & \mathbf{0} & \mathbf{0} \\ -a_4\left(\frac{2V_\infty}{c}\right)\mathbf{I} & a_3\left(\frac{2V_\infty}{c}\right)\mathbf{I} & \mathbf{0} \\ -a_5\left(\frac{2V_\infty}{c}\right)\mathbf{I} & \mathbf{0} & a_3\left(\frac{2V_\infty}{c}\right)\mathbf{I} \end{bmatrix} \tag{124}$$

$$\mathbf{K}_a = \begin{bmatrix} \mathbf{K}_0 + 0.5\mathbf{K}_1 + a_4\left(\frac{2V_\infty}{c}\right)\mathbf{C}_1 & \mathbf{K}_1 & \left(\frac{2V_\infty}{c}\right)\mathbf{C}_1 \\ -0.5a_2\left(\frac{2V_\infty}{c}\right)^2\mathbf{I} & a_2\left(\frac{2V_\infty}{c}\right)^2\mathbf{I} & \mathbf{0} \\ -a_6\left(\frac{2V_\infty}{c}\right)^2\mathbf{I} & \mathbf{0} & a_2\left(\frac{2V_\infty}{c}\right)^2\mathbf{I} \end{bmatrix} \tag{125}$$

$$\mathbf{F}_a = \begin{bmatrix} \mathbf{F} \\ \mathbf{0} \\ \mathbf{0} \end{bmatrix} \tag{126}$$

B. Example

For the example in Section 5, the wing has the following properties: $EI_{yy} = 1.2665 \times 10^4$ lb-ft^2, $GJ = 1.5880 \times 10^4$ lb-ft^2, $\rho A = 0.2313$ lb-sec^2/ft^2, $\rho I_{xx} = 0.0203$ lb-sec^2, $e = 0.2435c$, $e_c = 0.2565c$, $e_m = 0.0065$, and $e_{cg} = 0$. A 1% structural damping is assumed. A linear flutter analysis is performed for the cantilever boundary condition. The solution is approximated by the Galerkin method using the first four modes of a cantilever beam in bending and torsion. Figures16 and 17 show the frequency and damping of the wing as a function of the equivalent airspeed. The wing flutters at an equivalent airspeed of 296 ft/sec due to the first torsion (1T) mode at a frequency of 43.30 rad/sec exchanging energy with the first bending (1B) mode.

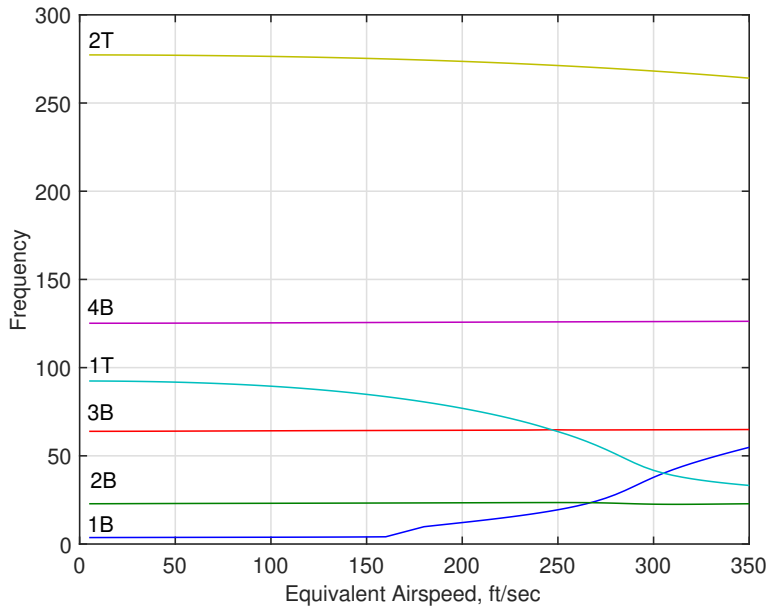

Figure 16. Frequency Vs. Equivalent Airspeed

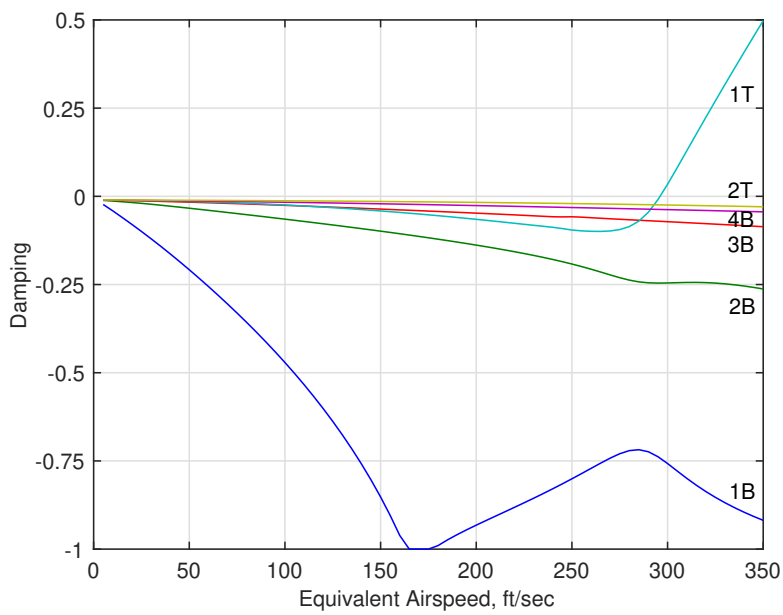

Figure 17. Structural Damping Vs. Equivalent Airspeed

A time simulation of the linear structural dynamic response analysis is then conducted at an equivalent airspeed of 300 ft/sec. The forcing function is a step change in the angle of attack by 0.1°. The linear structural dynamic responses of the bending deflection and torsional twist at the wing tip grow exponentially as shown in Figs. 18 and 19, respectively. Without accounting for structural failures due to the stress exceedance of the strength of the material, the responses grow exponentially due to instability.

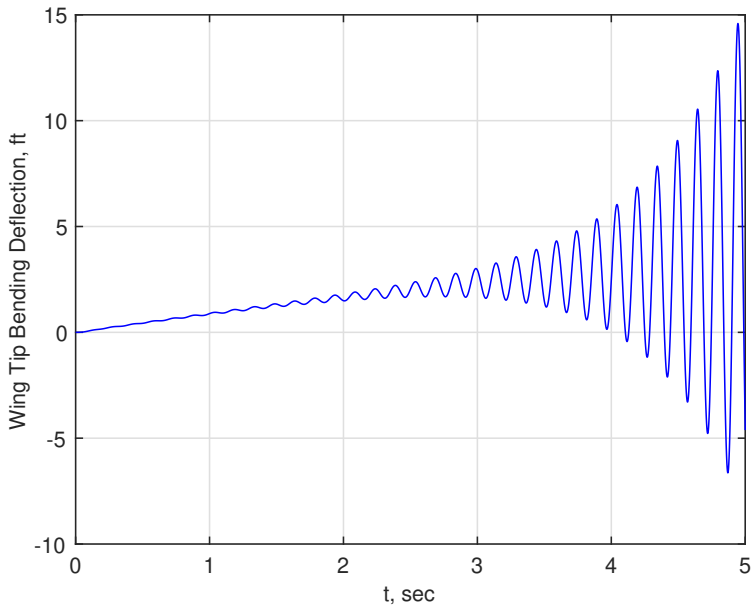

Figure 18. Response of Wing Tip Bending Deflection with Linear Theory

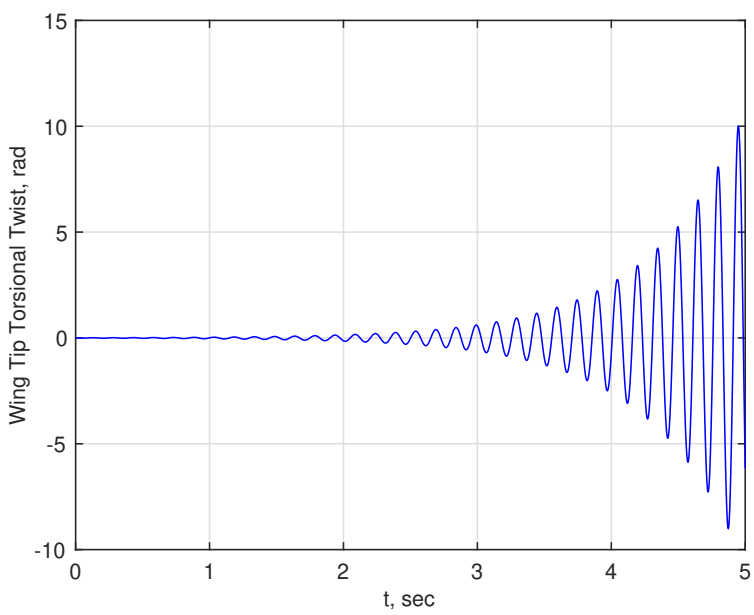

Figure 19. Response of Wing Tip Torsional Twist with Linear Theory

A nonlinear simulation due to the large deflection is performed next. Figures 20 and 21 show the nonlinear structural dynamic responses of the bending deflection and torsional twist at the wing tip. The responses shows a limit cycle oscillation (LCO) behavior after $t = 9$ sec which limits the exponential growth of the wing structural displacements. The The growth in the amplitudes of the bending deflection and torsional

twist is no longer present. The LCOs occur at a slightly lower frequency of about 40.80 rad/sec which is probably due to the increase in the nonlinear rotary inertia term $\rho I_{yy}\left(1+\frac{W_x^2}{2}\right)$ and the reduction in the apparent mass term $\frac{q_\infty \pi c^2\left(1-\frac{W_x^2}{2}\right)}{2V_\infty^2}$ in the bending mass. The solution is non-physical, however, because the bending deflection and torsional twist exceed reasonable deflection limits. This indicates a structural failure would occur before LCOs would set in.

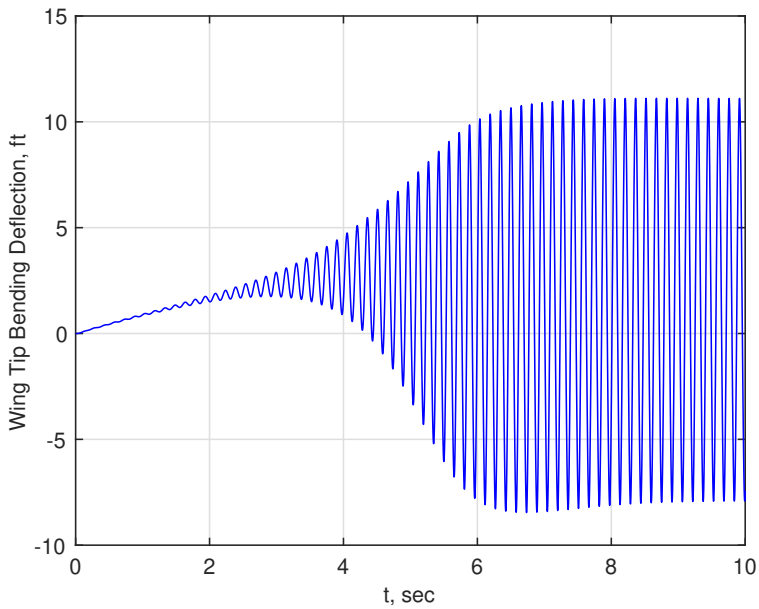

Figure 20. Response of Wing Tip Bending Deflection with Nonlinear Theory for $\alpha = 0.1°$

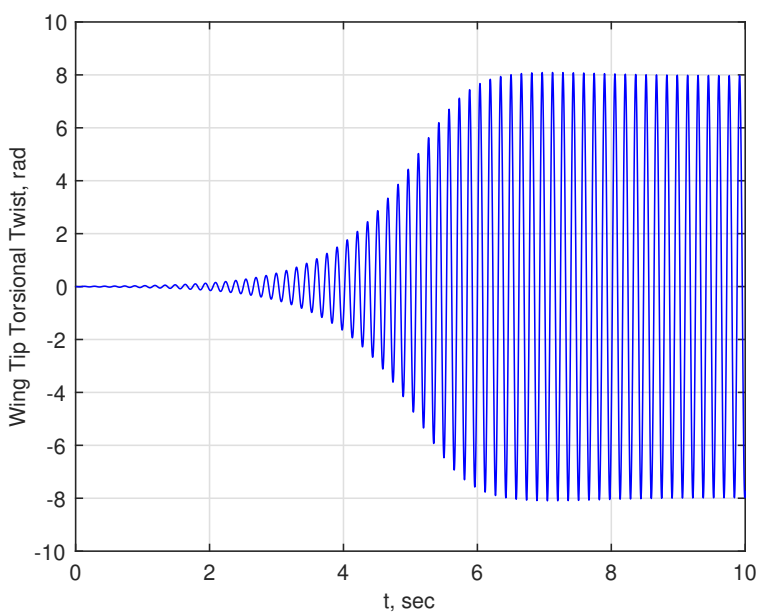

Figure 21. Response of Wing Tip Torsional Twist with Nonlinear Theory for $\alpha = 0.1°$

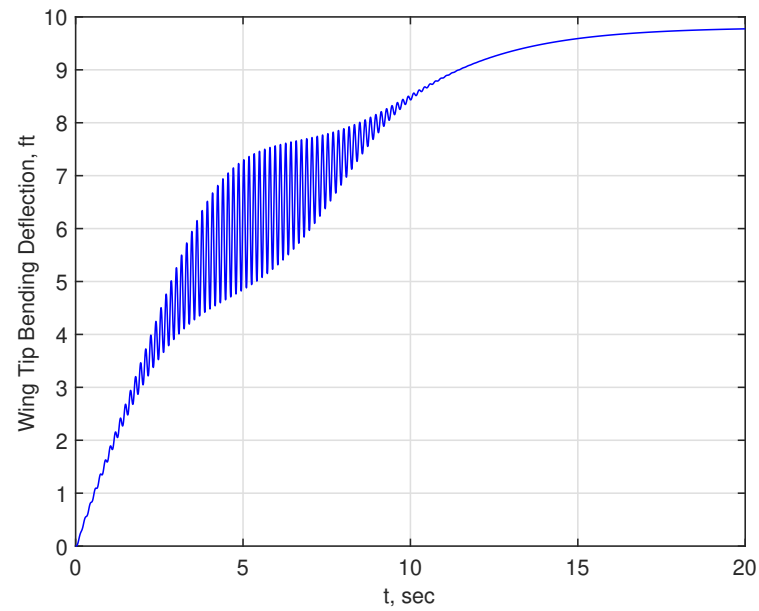

Figure 22. Response of Wing Tip Torsional Twist with Nonlinear Theory for $\alpha = 0.2°$

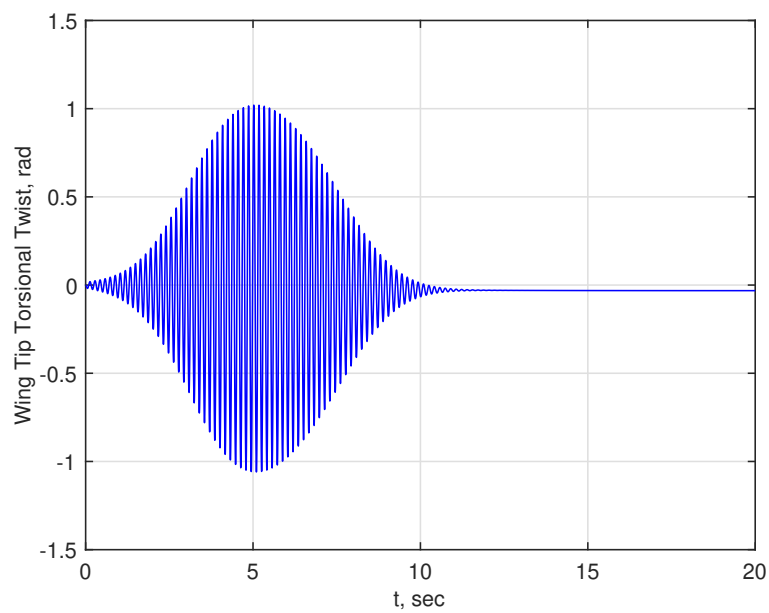

Figure 23. Response of Wing Tip Torsional Twist with Nonlinear Theory for $\alpha = 0.2°$

Because of the nonlinear nature of the structural dynamics, the amplitude of the excitation can change the LCO behavior drastically. To illustrate this, the forcing function is changed to a step input of 0.2° in

the angle of attack. Figures 22 and 23 shows the LCO behaviors of the structural dynamic response of the wing. The wing bending and torsion no longer exhibit a strong LCO behavior. The wing bending deflection exhibits initial transient oscillations and then reaches a steady state response. The wing torsion also exhibits a similar response with initial transient oscillations followed by a zero steady state response. The reduction in the LCO amplitude could probably be due to the nonlinear aerodynamic damping.

VII. Conclusions

This paper presents a theory on nonlinear large deflection aeroelasticity. The nonlinear bending theory properly accounts for the length preservation when the structure is not subject to axial loading. While the linear bending theory predicts a similar bending deflection characteristic, it does not account correctly for the axial displacement. As a result, the linear bending theory is not length-preserving. At smaller bending deflections, the length-preserving property may not be significant, but when the bending deflection is sufficiently large, the nonlinear bending theory predicts a reduction in the wing span whereas the linear theory would fail to predict this effect. As a result, this could cause a significant effect on the wing aerodynamic performance. A modified lifting line theory is developed to take into account the full deflection states of the wing deformation. An analysis is conducted via an example of a high aspect ratio unswept wing to illustrate the effect of nonlinear large deflection bending on aerodynamics based on the lifting line theory. The results show that the nonlinear bending deflection causes a reduction in lift and span efficiency factor. The induced downwash for the ideal elliptical lift distribution cannot remain uniform across the wing span due to the bending deflection.

The nonlinear large deflection effect on dynamic aeroelasticity is also examined. Flutter is a linear structural phenomenon which is due to the energy exchange between bending and torsion modes. As a structure approaches a flutter, the amplitudes of bending and torsion increase rapidly until the large deflection effect begins to set in to limit the amplitudes of the structural responses, thereby resulting in limit cycle oscillations. One possible mechanism of LCOs among many is due to the effect of the wing bending slope on the mass and damping of the structural dynamic modes.

Acknowledgment

The authors would like to acknowledge the Advanced Air Transport Technology Project under the Fundamental Aeronautics Program of NASA Aeronautics Research Mission Directorate (ARMD) for funding support of this work.

References

[1]Noll, T. E. and Eastep, F. E., "Active Flexible Wing Program," AIAA Journal of Aircraft, Vol. 32, No. 1, pp. 9-9, 1999.

[2]Pendleton, E., Flick, P., Voracek, D., Reichenbach, E., Griffin, K., and Paul, D., "The X-53,A Summary of the Active Aeroelastic Wing Flight Research Program," AIAA Structures, Structural Dynamics, and Materials Conference, AIAA-2007-1855, Honolulu, HI, April, 2007.

[3]Nguyen, N., "Elastically Shaped Future Air Vehicle Concept," NASA Innovation Fund Award 2010 Report, October 2010, Submitted to NASA Innovative Partnerships Program, http://ntrs.nasa.gov/archive/nasa/casi.ntrs.nasa.gov/20110023698.pdf.

[4]Nguyen, N., Trinh, K., Reynolds, K., Kless, J., Aftosmis, M., Urnes, J., and Ippolito, C., "Elastically Shaped Wing Optimization and Aircraft Concept for Improved Cruise Efficiency," 51st AIAA Aerospace Sciences Meeting, AIAA-2013-0141, January 2013.

[5]Urnes, J., Nguyen, N., Ippolito, C., Totah, J., Trinh, K., and Ting, E., "A Mission Adaptive Variable Camber Flap Control System to Optimize High Lift and Cruise Lift to Drag Ratios of Future N+3 Transport Aircraft," 51st AIAA Aerospace Sciences Meeting, AIAA-2013-0214, January 2013.

[6]Nguyen, N. and Urnes, J., "Aeroelastic Modeling of Elastically Shaped Aircraft Concept via Wing Shaping Control for Drag Reduction," AIAA Atmospheric Flight Mechanics Conference, AIAA-2012-4642, August 2012.

[7]Nguyen, N. and Ting, E., "Inertial Force Coupling to Nonlinear Aeroelasticity of Flexible Wing Aircraft," AIAA Dynamics Specialists Conference, AIAA-2016-1094, January 2016.

[8]Chaparro, D., Fujiwara, G., Ting, E., and Nguyen, N., "Aerodynamic Modeling of Transonic Aircraft Using Vortex Lattice Coupled with Transonic Small Disturbance for Conceptual Design," 34th AIAA Applied Aerodynamics Conference, AIAA-2016-3012, June 2016.

[9]Fujiwara, G., Chaparro, D., and Nguyen, N., "An Integral Boundary Layer Direct Method Applied to 2D Transonic Small-Disturbance Equations," 34th AIAA Applied Aerodynamics Conference, AIAA-2016-3160, June 2016.

[10]Nguyen, N., Ting, E., Nguyen, D., Dao, T., and Trinh, K., "Coupled Vortex-Lattice Flight Dynamic Model with Aeroe-

lastic Finite-Element Model of Flexible Wing Transport Aircraft with Variable Camber Continuous Trailing Edge Flap for Drag Reduction," AIAA Atmospheric Flight Mechanics, AIAA-2013-4746, August 2013.

[11]Nguyen, N., "Integrated Flight Dynamics Modeling of Flexible Aircraft with Inertial Force-Propulsion - Aeroelastic Couplings," 46th AIAA Aerospace Sciences Meeting and Exhibit, AIAA-2008-0194, Reno, NV, January 2008.

[12]Houbolt, J. C. and Brooks, G. W., "Differential Equations of Motion for Combined Flapwise Bending, Chordwise Bending, and Torsion of Twisted Nonuniform Rotor Blades," NACA Technical Note 3905, February 1957.

[13]Hodges, D. W., "Proper Definition of Curvature in Nonlinear Beam Kinematics," AIAA Journal, Vol. 22, No. 12, 1984, pp. 1825-1827.

[14]Monasa, F. and Lewis, G., "Large Deflections of Point Loaded Cantilevers with Nonlinear Behavior," Journal of Applied Mathematics and Physics (ZAMP), Vol. 34, January 1983, pp. 124-130.

[15]Reddy, J. N. and Singh, I. R., "Large Deflections and Large-Amplitude Free Vibrations of Straight and Curved Beams," International Journal for Numerical Methods in Engineering, Vol. 17, 1981, pp. 829-852.

[16]Nguyen, N. T., Ting, E., and Chaparro, D., "Nonlinear Large Deflection Theory with Modified Aeroelastic Lifting Line Aerodynamics for a High Aspect Ratio Flexible Wing," 35th AIAA Applied Aerodynamics Conference, AIAA-2017-4219, June 2017.

[17]Anderson, J. D., *Fundamentals of Aerodynamics*, 2nd Edition, McGraw-Hill, 1991.

[18]Nguyen, N., Ting, E., and Lebofsky, S., "Aeroelasticity of Axially Loaded Aerodynamic Structures for Truss-Braced Wing Aircraft," 56th AIAA/ASME/ASCE/AHS/ASC Structures, Structural Dynamics, and Materials Conference, AIAA-2015-1840, January 2015.

[19]Vassberg, J. C., DeHaan, M. C., Rivers, S. M., and Wahls, R. A., "Development of a Common Research Model for Applied CFD Validation Studies," AIAA Applied Aerodynamics Conference, AIAA 2008-6919, August 2008.

[20]Miranda, L. R., Elliott, R. D., and Baker, W. M., "A Generalized Vortex Lattice Method for Subsonic and Supersonic Flow Applications," NASA Contractor Report 2865, December 1977.

[21]Drela, M., "A User's Guide to MSES 3.05," MIT Department of Aeronautics and Astronautics, July 2007.